NATIONAL TECHNICAL UNIVERSITY OF ATHENS
SCHOOL OF NAVAL ARCHITECTURE AND MARINE ENGINEERING
M.Sc. MARINE TECHNOLOGY AND SCIENCE
OCEAN AND COASTAL TECHNOLOGY

Master's Thesis

"Polarization curves modelling concerning the corrosion behavior of naval steels and experimental validation"

Rachel S. Tsoutsani

Thesis Examination Committee

Professor D. I. Pantelis, Supervisor
Professor D. E. Manolakos
Professor N. G. Tsouvalis

Athens, January 2016

“Polarization curves modelling concerning the corrosion behavior of naval steels and experimental validation”

AKNOWLEDGEMENTS

This M.Sc. thesis would not have been possible without the support of many people. I would like to express my gratitude to my supervisor-Professor D.I. Pantelis, who was extremely helpful and offered invaluable assistance, support and guidance.

Moreover, I would like to thank Mrs. D. Tsiourva, Chemical Engineer and Ass. Professor A. Karantonis for their guidance and valuable help in the achievement of this work.

Finally, I would like to extend my thanks to my family for supporting and understanding me throughout all my years of studies, and to my friends who have always been there.

ΠΕΡΙΛΗΨΗ

Η παρούσα διπλωματική εργασία ασχολείται με τη χρήση του χάλυβα στη ναυπηγική βιομηχανία και συγκεκριμένα με το φαινόμενο της διάβρωσης χάλυβα AH36 και S690 σε διάλυμα NaCl 3.5% κ.β. ώστε να προσομοιωθούν οι συνθήκες θαλάσσιου περιβάλλοντος. Εκπονήθηκε στο εργαστήριο Ναυπηγικής Τεχνολογίας της Σχολής Ναυπηγών Μηχανολόγων Μηχανικών του ΕΜΠ.

Η αποτίμηση της προδιάθεσης για διάβρωση των χαλύβων έγινε πειραματικά χρησιμοποιώντας τη μέθοδο ηλεκτροχημικής πόλωσης (Μέθοδος προεκβολής ευθειών Tafel) και με την ανάπτυξη μοντέλου ηλεκτροχημικής πόλωσης με την χρήση του λογισμικού Comsol Multiphysics 4.3b. Τα αποτελέσματα της μοντελοποίησης αξιολογούνται σύμφωνα με τα πειραματικά δεδομένα.

Σκοπός της εργασίας είναι η σύγκριση των δύο χαλύβων ως προς την αντοχή τους σε διάβρωση καθώς και η σύγκριση των πειραματικών αποτελεσμάτων με αυτά της μοντελοποίησης ώστε να αξιολογηθεί η αξιοπιστία της προσομοίωσης του πειράματος.

ABSTRACT

.

This thesis deals with the use of steel in shipbuilding industry and in particular with the corrosion of AH36 and S690 steel in marine environment (solution NaCl 3.5% w/w). The experimental procedure is prepared in the Shipbuilding Technology Laboratory, School of Naval Architecture and Marine Engineering, NTUA.

The predisposition for corrosion was investigated experimentally by polarization methods (Linear Polarization and Tafel method) as well as by developing a finite element model using Comsol Multiphysics 4.3b software. The results of the modeling will be evaluated with experimental data.

The purpose of this thesis is the comparison of the two steels regarding their resistance to corrosion as well as the evaluation of the simulation method concerning the verification of simulating the experimental investigation.

TABLE OF CONTENTS

TABLE OF FIGURES

1. CORROSION

1.1 Introduction

Corrosion is the breakdown of materials. Especially, it stands for material deterioration or surface damage in an aggressive environment. Steel corrosion is a chemical or electrochemical oxidation process, in which the metal transfers electrons to the environment and undergoes a valence change from zero to a positive value.

The environment may be liquid, gas or hybrid soil-liquid. These environments are called electrolytes since they have their own conductivity for electron transfer.

1.1.1 Significance of corrosion [12][18]

Corrosion interfere itself into many parts of our lives. The majority of us have a personal feeling for the definition and importance of corrosion. The outdoor rusting of steel house and garden appliances, expensive repairs to home plumbing systems and the water lines serving our homes, stains on cooking utensils or the metallic taste in acid food stored too long in opened cans, are some examples of corrosion which is met in our daily life.

Moreover, we are all familiar with many of the measures taken to combat corrosion. Hundreds of dollars have been spent on aftermarket corrosion protection systems so as to delay the dreaded rust appearance. The economic costs of corrosion in the United States of America alone have been estimated between $8-$126 billion per year. The most comprehensive study on the economic cost of corrosion in the United States, performed in 1976, estimated an annual cost of $70 billion. Some measures, while reducing corrosion will cost more than the parts or the equipment protected. Nevertheless, the economic costs of corrosion are obviously enormous.

Some of the most important indirect costs of corrosion are summarized as follows:

1. Plant Downtime: Parts and labor to replace corroded equipment are often minor compared to the loss of production while the plant is inoperable during repairs. For example, the cost to replace power from a shutdown nuclear power plant can run into millions of dollars per day.
2. Loss of Product: Leaking containers, tanks and pipelines result a significant losses in product, which have a high cost. These leaks and spills have a corresponding hazardous effect on the surrounding environment and safety of the populace. Thousands of leaking automotive service station fuel tanks must be repaired or replaced to prevent recurring losses of fuel and contamination of groundwater. The expense is enormous, with an impact on the livelihood of many independed stations operators.
3. Loss of Efficiency: Accumulated corrosion products on heat exchanger tubing and pipelines decrease the efficiency of heat transfer and reduce the pumping capacity, respectively.
4. Contamination: Soluble corrosion products can spoil chemical preparations of soap, dyes, and pharmaceuticals, among others. A major problem in many nuclear power generating plants is the transport of radioactive corrosion products from the reactor core followed by deposition in other parts of the cooling water system, necessitating dangerous and expensive shutdowns to decontaminate. In time past, lead pipes released toxic corrosion products into soft waters for public consumption. Fortunately, lead has long been prohibited from use in this application.
5. Overdesign: In absence of adequate corrosion rate information, overdesign is required to ensure reasonable service life, resulting in wasted resources, and greater power requirements for moving parts. Engineers sometimes overdesign through ignorance of available information which may not be available, however. Geologic storage of high-level nuclear waste in deep repositories, mandated by the U.S. Congress, requires containers that will maintain their integrity for 300 to 1000 years. Corrosion data in environments resembling the relevant groundwaters in radiation fields at elevated temperature are not available and are currently being generated in extensive test programs. However, extrapolations of such data, gathered in a few years at most, are highly uncertain, and considerable overdesign will almost certainly be included.

Were it not so insidious and ubiquitous, corrosion could be classified collectively as the greatest economic calamity known to humankind. As a result, corrosion is the root of many individual economic calamities.

For all the above mentioned reasons, reliable prediction of corrosion initiation and propagation would be a good basis for cost-effective maintenance and repair strategies. The development of reliable models and simulations is an essential part of future predictive maintenance concepts. They would deliver the information about onset and evolution of corrosion and fill the gap between corrosion detection or monitoring and estimation of its structural impact.

Corrosion testing is known to be extremely time consuming. Corrosion prediction models are going to save marine development and implementation costs via minimization of testing. The prediction models can be combined with expert systems and databases to allow a more efficient and reliable materials selection.

1.1.2 Definition of corrosion [13][17][20]

Corrosion can be defined as the deterioration of a metallic material's properties due to its interaction with its environment. Specifically, is a chemical or electrochemical oxidation process, in which the metal transfers electrons to the environment and undergoes a valence change from zero to a positive value. The environment may be liquid, gas or hybrid soil-liquid. These environments are called electrolytes since they have their own conductivity for electron transfer.

An electrolyte is analogous to a conductive solution, which contains positively and negatively charged ions called cations and anions, respectively. An ion is an atom that has lost or gained one or more outer electron and carries an electrical charge. Thus, the corrosion process which can be chemical in nature or electrochemical due to a current flow requires at least two reactions that must occur in a particular corrosive environment. These reactions are classified as anodic and cathodic reactions and are defined below for a metal Fe immersed in NaCl 3.5% acid solution as an example. Hence, metal oxidation occurs through an anodic reaction and reduction is through the cathodic reactions as shown below:

$$\text{Fe} \rightarrow Fe^{2+} + 2e^{-} \qquad \text{Anodic - Oxidation} \qquad (1.1)$$

$$2H^{+} + 2e^{-} \rightarrow H_2 \qquad \text{Cathodic - Reduction} \qquad (1.2)$$

$$O_2 + 2H_2O + 4e^{-} \rightarrow 4OH^{-} \qquad \text{Cathodic - Reduction} \qquad (1.3)$$

The explanation of these equations indicate that an anodic reaction, which is also referred to as an oxidation reaction, loses electrons which has been gained by the cathodic reaction for producing ions into the electrolyte and the cathodic reaction which is equivalent to a reduction reaction, accepts or gains electrons for reducing pertinent ions. Consequently, both anodic and cathodic reactions are coupled in a corrosion process. The arrows in the previous reactions indicate the reaction directions as written and they represent irreversible reactions.

The concepts of metal oxidation and metal reduction or electrode position are schematically shown in *Figure 1*.

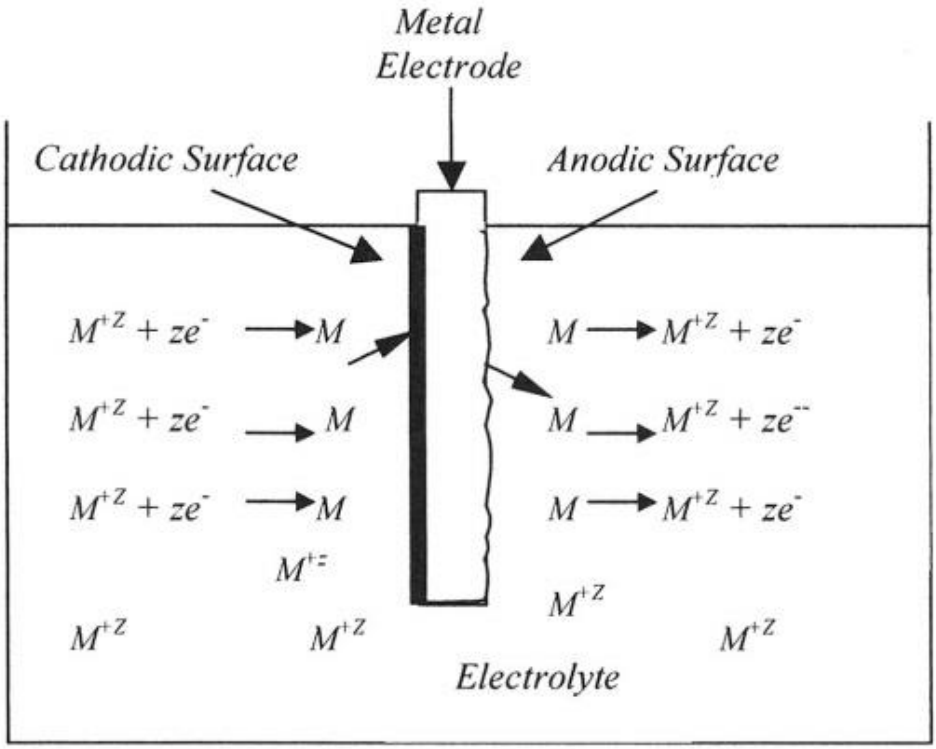

Figure 1: Schematic electrochemical cell [17]

The dark thick line on the metal electrode is a representation of metal deposition as a result of metal ion reduction and metal oxidation is shown on the left-hand side of the electrode.

1.1.3 Oxidation and Reduction of Alloys [8][13][17]

Redox (Reduction & Oxidation) reactions include all chemical reactions in which atoms have their oxidation state changed. In general, redox reactions involve the transfer of electrons between species.

- **Oxidation** is the loss of electrons or an increase in oxidation state by a molecule, atom, or ion.
- **Reduction** is the gain of electrons or a decrease in oxidation state by a molecule, atom, or ion.

In Redox reactions, an oxidation reaction happens simultaneously at a reduction reaction. The oxidation alone and the reduction alone are each called a half-reaction, because two half-reactions always occur together to form a whole reaction. When writing half-reactions, the gained or lost electrons are typically included explicitly in order that the half-reaction be balanced with respect to electric charge.

Oxidation and reduction properly refer to a change in oxidation state while the actual transfer of electrons may never occur. Thus, oxidation is better defined as an increase in oxidation state, and reduction as a decrease in oxidation state. In practice, the transfer of electrons will always cause a change in oxidation state, but there are many reactions that are classed as "redox" even though no electron transfer occurs (such as those involving covalent bonds).

There are simple redox processes, such as the oxidation of carbon to yield carbon dioxide (CO_2) or the reduction of carbon by hydrogen to yield methane (CH_4), and more complex processes such as the oxidation of glucose ($C_6H_{12}O_6$) in the human body through a series of complex electron transfer processes.

If the reducing state is at physical contact with the oxidant state, the transfer of electrons is direct. Nevertheless, when they are in electrical contact, there is electricity production, namely the chemical power is converted into electrical power (galvanic cell). Having an external source of electrical power, the above reaction is reversed and as a result the electrical power is converted into chemical power (electrolysis).

1.2 Classification of corrosion [7][12][18]

There is not a unique classification of the types of corrosion, but the following classification is adapted hereafter.

1.2.1 General corrosion

In general corrosion, the exposed metal/alloy surface area is entirely corroded in an environment such as a liquid electrolyte (chemical solution, liquid metal), gaseous electrolyte (air, CO_2, etc.), or a hybrid electrolyte (solid and water, biological organisms, etc.). Some types of general corrosion and their description are given below:

- **Uniform Corrosion** is the usually expected mode of corrosion. The corrosive environment must have the same access to all parts of the metal surface and the metal itself must be metallurgically and compositionally uniform. Atmospheric corrosion is probably the most prevalent example of uniform corrosion at a visually apparent rate. Generally, uniform corrosion is preferred from a technical viewpoint because it is predictable and thus acceptable for design.
- **Galvanic Corrosion** is either a chemical or electrochemical corrosion which may arise when two dissimilar metals are in contact in an aqueous environment. The potential difference between them will initiate attack at a corrosion rate that is largely dependent upon the surface reactions of the two metals.
- **Environmentally Induced Cracking** is separated into three types of failure. Stress corrosion cracking occurs in alloys with a static tensile stress in the presence of specific environmental conditions. Corrosion fatigue occurs under cyclic stresses in a corrosive environment and hydrogen induced cracking is caused by hydrogen diffusing into the alloy lattice when the hydrogen evolution reaction produces atomic hydrogen at the surface during corrosion, cleaning and pickling or cathodic protection.
- **Intergranular Corrosion** Reactive impurities may segregate or passivating elements such as chromium may be depleted at the grain boundaries. As a result, the grain boundary or adjacent regions are often less corrosion resistant and preferential corrosion at the grain boundary may be severe

enough to drop grains out of the surface. Hence, Intergranular Corrosion is a common problem in many alloy systems.

- **Erosion – Corrosion** is the combination of a corrosive fluid and high flow velocity. The same stagnant or slow-flowing fluid will cause a low or modest corrosion rate, but rapid movements of the corrosive fluid physically erodes and removes the protective corrosion product film, exposes the reactive alloy beneath and accelerate erosion-corrosion attack.
- **High – Temperature Corrosion** is a mechanism of corrosion that takes place in gas turbines, diesel engines, furnaces, or other machinery coming in contact with hot gas containing certain contaminants. Fuel sometimes contains vanadium compounds or sulfates which can form compounds during combustion having a low melting point. These liquid melted salts are strongly corrosive for stainless steel and other alloys normally inert against the corrosion and high temperatures.
- **Liquid - Metal Corrosion** is a phenomenon of practical importance, where certain ductile metals experience drastic loss in tensile ductility or undergo brittle fracture when tested in the presence of specific liquid metals.
- **Molten – Salt Corrosion.** Molten salts can be quite corrosive at high temperatures with corrosion being driven by thermodynamics, impurity effects, and activity and temperature gradients. Understanding and mitigating materials corrosion in these molten salt environments by appropriate materials selection and salt chemistry control are necessary for their effective implementation in nuclear energy systems.
- **Biological Corrosion or Biocorrosion** is the deterioration of metals as a result of the metabolic activity of microorganisms.
- **Stray - Current Corrosion** refers to corrosion resulting from stray current - current flowing through paths other than the intended circuit. The process of stray current corrosion is electrolysis in nature. The extent of damage or loss of metal is directly proportional to the magnitude of stray current passing through the system.

1.2.2 Localized corrosion [7][12][18]

Localized corrosion can be described as a corrosion which occurs at specific parts of an exposed surface area. This form of corrosion is more difficult to control than general corrosion. While localized corrosion may not consume as much material, penetration and failure are often more rapid. Localized corrosion can be classified as:

- **Crevice Corrosion:** Corrosion of an alloy is often greater in the small sheltered volume of the crevice created by contact with another material. The second material may be part of a fastener (bolt, rivet, washer) of the same or a different alloy, a deposit of mud or other insoluble solid. Corrosion within a crevice may be caused in atmospheric exposures by detention of water, while the outer surfaces can drain and dry.
- **Filiform Corrosion** is basically a special type of crevice corrosion, which occurs under a protective film. It is common on food and beverage cans being exposed to the atmosphere.
- **Pitting Corrosion** is an extremely localized corrosion mechanism. It is associated with the breakdown of a film and it occurs on a completely flat surface. The pits may be deep, shallow or undercut. Pitting shares the same mechanism with crevice corrosion in stainless steels.
- **Oral Corrosion** occurs on dental alloys exposed to saliva.
- **Biological Corrosion** due to fouling organisms non-uniformly adhered on steel in marine environments.
- **Selective Leaching Corrosion** is a metal removal process from the base alloy matrix, such as dezincification (Zn is removed) in Cu-Zn alloys and graphitization (*Fe* is removed) in cast irons.

The *Figure 2* below, pictures various forms of corrosion:

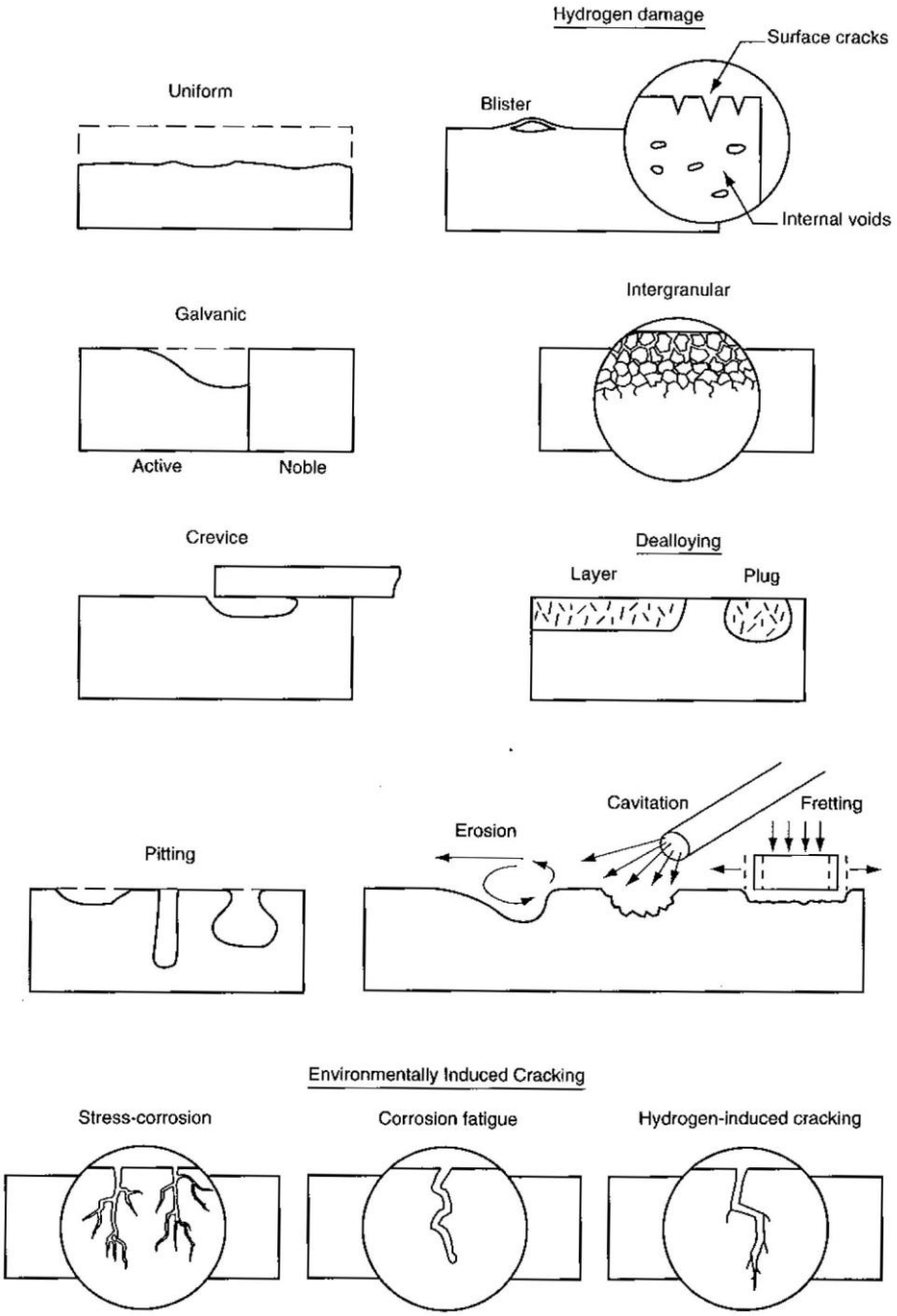

Figure 2: Schematic summary of the various forms of corrosion [18]

1.3 Corrosion of steel [1][9][11][19][24]

Steel is among the most widespread construction and building materials because of its high tensile strength and low costs. Its industrial use as building material began in the late 19th century. It is a material with excellent mechanical properties. The high tensile strength and compressive strength make it an ideal material for a wide range of structures from surgical tools to aerospace and shipbuilding.

The deterioration of mechanical properties is predominant in the design of steel structures. The most common material used in ship structures is steel because of its high tensile strength and low cost. Steel derives its mechanical properties from a combination of chemical composition.

The major constituent of steel is alloys of iron (Fe) and other elements, primarily carbon alloy which contributes up to 2.1% of its weight. Varying the amount of alloying elements their formation in the steel either as solute elements, or as precipitated phases, retards the movement of those dislocations that make iron comparatively ductile and weak, and thus controls qualities such as the hardness, ductility, and tensile strength of the resulting steel. Steel's strength compared to pure iron is only possible at the expense of ductility, of which iron has an excess.

Usually, pure metals are more resistant to corrosion comparing to them who consist of different types and quantities of alloys. However, pure metals are soft and have low mechanical properties. Thus they are used in a few and specialized cases.

The present thesis deals with the corrosion behavior of AH36, common structural steel in shipbuilding industry, in comparison with S690 steel, high strength low alloy steel (HSLA), which consists a promising alternative for structural parts in shipbuilding.

In the following paragraphs, detailed description of each of these steels is presented.

1.3.1 AH36 (High Strength) Steel [11][17][19]

AH36 steel is the most common structural steel in shipbuilding industry owing to its low corrosion susceptibility and suitable mechanical properties. Regarding the AH36 steel, ferritic-pearlitic microstructure was observed. Its designation is according to A131M standard of ASTM and comes from Lloyd's Register of Shipping Steels. However, in some countries this steel is encountered with different name such as K11852 in U.S.A, A36 in Russia, 1.0565 in Germany etc. The yield point of AH36 steel is 36 Kp/mm^2 or 353.2 MPa and its hardness is approximately 180 Vickers. The Chemical composition and Mechanical properties of AH36 steel are presented in the *Figure 3* & *Figure 4* below:

Chemical Composition	%
C	0.180
Mn	0.90-1.60
Si	0.10-0.50
P	0.035
S	0.035
Al (sid)	0.015
Cu	0.350
Cr	0.200
Ni	0.400
Mo	0.080
Nb	0.050
V	0.100
Ti	0.020

Figure 3: Chemical characteristics of AH36 high tensile steel. [11]

Mechanical characteristics	
Tensile Strength (MPa)	490-630
Yield Strength (MPa)	355
% Elongation in 2 in. (50 min)	21
Impacting Test Temperature	0

Figure 4: Mechanical properties of AH36 high tensile steel according to IACS (International Association of Classification Societies) [11]

1.3.1.1 Use of AH36 steel

The most recent years there is an increasing use of AH36 steel because the plate thickness is reduced and it has lower weight than other steels. Nowadays AH36 is almost exclusively utilized in the shipbuilding industry for the construction of structural parts of ships such as side shell, side shell frame, bulkhead, bottom plate, inner bottom plate, and longitudinal members.

The hull and the tanks of the ships are usually made from common shipbuilding steel. However, in recent years the use of high strength steels expands. The result of this use is thinner and lower weight sheets, compared to carbon steels.

Compared with common mild steel, the high-strength steel AH36 presents:

- Lower carbon content
- Higher hardness values
- Higher strength
- Same resistance to fatigue
- Same good weldability
- Higher resistance to corrosion

In high-strength steel there are greater stresses (due to reduced thickness) so, the abrasion of protective coatings is made faster, thus increasing the likelihood of crack initiation and therefore the risk of stress corrosion cracking.

1.3.2 S690 (High Strength Low Alloy) Steel [1][22][24][25]

The use of higher strength steels allows the design of lighter, slenderer and simpler structures. High-strength, low-alloy (HSLA) steels, like S690 have yield and tensile strengths that are two to three times higher than structural steels commonly considered in design codes, typically S235 and S355 steels. The 'S', in front of the number, stands for Structural steel.

High Strength Low Alloy (HSLA) steels have been developed since the 1960s originally for large diameter oil and gas pipelines. The requirement was high strength as compared to mild carbon steel, combined with improved toughness and good weldability. The S690 steel, as an HSLA steel, is a combination of ferrite and bainite. The yield point of S690 steel is 578 MPa and its hardness is approximately 280 Vickers. The Chemical composition and Mechanical properties of HSLA S690 are presented in the figures below (*Figure 5*, *Figure 6*):

Chemical Composition	%
C	0.200
Mn	1.700
Si	0.800
P	0.025
S	0.015
Al	0.015
Nb	0.060
V	0.120
Ti	0.050
Cu	0.500
Cr	1.500
Ni	2.000
Mo	0.700
B	0.005
Zr	0.150

Figure 5: Chemical characteristics of S690 steel [25]

Mechanical characteristics	
Young modulus (MPa)	206.30
Ultimate tensile stress (MPa)	730.50
Yield stress (MPa)	578
Strain at break (%)	35
Cyclic Young modulus (MPa)	214
Cyclic strain hardening coefficient (MPa)	978
Cyclic strain hardening exponent (MPa)	0.112

Figure 6: Tensile and cyclic properties of S690 steel [25]

1.3.2.1 Use of S690 steel

HSLA S690 steel is widely used in the lightweight design of lifting cranes, ground vehicles, construction equipment, high speed ships and numerous other applications for which an increase in strength, allows for larger scale structures that could not be attained with standard steels. The ship building industry is looking to higher strength steels in order to develop lighter and more fuel efficient ships with S690 type grades being the highest strength of the series of grades under consideration.

S690 steel presents improved fatigue crack initiation and crack arrest properties, compared to conventional marine steels. The fatigue crack growth property is reported to be superior to that of conventional steel because it possesses an optimum ferrite and bainite dual phase microstructure and the dual phase boundaries reduce fatigue crack growth.

Some of the advantages of HSLA among ordinary carbon steels are:

- Much stronger and tougher
- Ductile
- Highly formable
- Weldable
- Highly resistant to atmospheric corrosion - which is important since the structure may be in place for a long time.

2. ELECTROCHEMISTRY [2][7][13][15]

2.1 Definitions

«It is a common point of view that the chemical nature and structure of the surface of a metal, which is in contact with an electrolyte, are decisive in the kinetics of electrochemical reactions that proceed on this surface.»
Pletnev in regards to the corrosion of iron by chlorides in acidic media.

This "common point of view" is manifested in the great body of work in corrosion science that proposes mechanisms that explain how corrosion reactions occur. Corrosion in aqueous environments proceeds via an electrochemical mechanism, in which the coupled anodic and cathodic reactions take place at unique sites within the material/environment interface. The reactions themselves involve transfer of electrons or ions—often both—across the electrochemical double layer.

Corrosion of metals is, most of the time, electrochemical reaction. This reaction involves movement of electrons and it needs either energy consumption so as to occur or it is itself the source of this energy.

2.2 Electrochemical nature of aqueous corrosion

Nearly all metallic corrosion processes involve transfer of electronic change in aqueous solutions. Thus, it is necessary to discuss the electrochemical nature of corrosion.

Aqueous corrosion can take many forms. Apart from general corrosion which results in a relatively uniform removal of a surface, specific features in a metal surface may be preferentially or selectively attached. Such features include grain boundaries, precipitates and metal/inclusion interfaces. The presence of films on a metal surface may give rise to highly localized regions of corrosion attack, resulting, maybe, in pitting. With all these forms of corrosion an anodic and a cathodic reaction must occur, for it was established many years ago that metals corrode in aqueous environments by an electrochemical mechanism. When a piece of metal is corrodes

there are anodic and cathodic sites. These may be permanently separated from each other, but in many cases the whole metal surface consists of anodic and cathodic sites which are continually shifting. At an anodic site an oxidation process occurs, which is a loss of electrons, and the metal goes into solution by reaction that can be depicted as:

$$\text{Fe} - 2e^- \rightarrow Fe^{2+}$$

For this reaction to take place a simultaneous process, which is a gain of electrons, must occur at a cathodic site. This reaction consumes those electrons provided by the oxidative process. Unless these electrons can be consumed, then the anodic reaction cannot occur. The reduction of dissolved oxygen and the liberation of hydrogen gas by the reduction of hydrogen ions are the two most common reactions occurring during the aqueous corrosion of metals. These can be depicted as:

$$O_2 + 4e^- + 2H_2O \rightarrow 4OH^-$$

$$2H^+ + 2e^- \rightarrow H_2$$

2.3 Chemical vs. electrochemical reactions [18][19][20]

Chemical reactions are those in which elements are added or removed from a chemical species. Purely chemical reactions are those in which none of the species undergoes a change in its valence. Electrochemical reactions are chemical reactions in which not only may elements be added or removed from a chemical species but also at least one species undergoes a change in the number of valence electrons.

For example, the precipitation of iron hydroxide, $\text{Fe}(OH)_2$, is a pure chemical reaction:

$$Fe^{2+} + 2OH^- \rightarrow \text{Fe}\,(OH)_2$$

None of the atoms involved have changed its valence, the iron and oxygen are still in the divalent state, and the hydrogen is still univalent. One way to produce the ferrous ion needed in the above reaction is via the oxidation of metallic (zero valent) iron:

$$Fe \rightarrow Fe^{2+} + 2e^{-}$$

In order for this reaction to occur, the two electrons produced must be consumed in a reduction reaction such as the reduction of dissolved oxygen:

$$O_2 + 2H_2O + 4e^{-} \rightarrow 4OH^{-}$$

If the two reactions are not widely physically separated on a metal surface, the chemical reaction between the hydroxide and ferrous ions can produce a solid on the surface. Thus chemical and electrochemical reactions can be coupled as it happens very often.

The most basic characteristics of electrochemical reactions and the differences with the chemical are the followings:

- They are always heterogeneous, whilst chemical reactions are either homogeneous or heterogeneous
- During an electrochemical reaction is produced or consumed electrical power. At a chemical reaction the absorbed or generated energy is thermal, luminous etc.
- The production of products occurs in the electrode area, while at electrical reaction, products are produced in various parts of the system.
- The products of electrochemical reactions are free from parasitic impurities. The products of electrical ones which are made by thermal stimulation are not free.
- Increasing the capacity within 1V the speed of electrochemical reaction is increased by a factor of 10^{10}. At a chemical reaction, to increase the speed at 10^3 the temperature has to be increased to 200^{o}C.
- An electrochemical action effected by passage of electrical current. Electrons removed from the system or coming into the system from outside. However, the movement of electrons in chemical reactions takes place randomly in space and their transfer becomes from one reaction to another.

2.4 Electrochemical cells [18][20][7]

An electrochemical system can be classified into three categories (*Figure 7*):

- **Galvanic cell** is formed when two dissimilar metals are connected electrically while both are immersed in a solution electrolyte. This electrochemical event produces electric energy from the stored chemical energy in the metallic anode. Hence, current flows from the cathode to the anode through the metallic circuit and electric power P=EI is produced.
- **Electrolytic cell** in which the source of power is external. Because of the external source the (-) of anode becomes (+) and the (+) of cathode (-). This cell consumes power, P = EI, and the cell reactions are driven in the reverse direction as opposed to galvanic, that is, the galvanic spontaneous reactions are driven backwards. This is possible if the applied potential is greater than the galvanic potential. This type of cell is very useful in the electrometallurgy field for recovering metals from oxide ores by electroplating the metal ions on cathodes. Hence, if current flows, then the principles of electrochemical stoichiometry are used for producing electrochemical reactions through the process of electrolysis and metal ions are deposited on a cathode surface.
- **Concentration cell** has mono-metallic electrodes, but the anode is immersed in a concentrated region of the electrolyte. The electrodes are made of the same metal and this cell is similar to a galvanic with respect to the electrode polarity and current flow direction. The electrodes are immersed in a nonhomogeneous electrolyte, but the anode is within the concentrated portion of the electrolyte where the concentration of species j is $C_j(anode) > C_j(cathode)$.

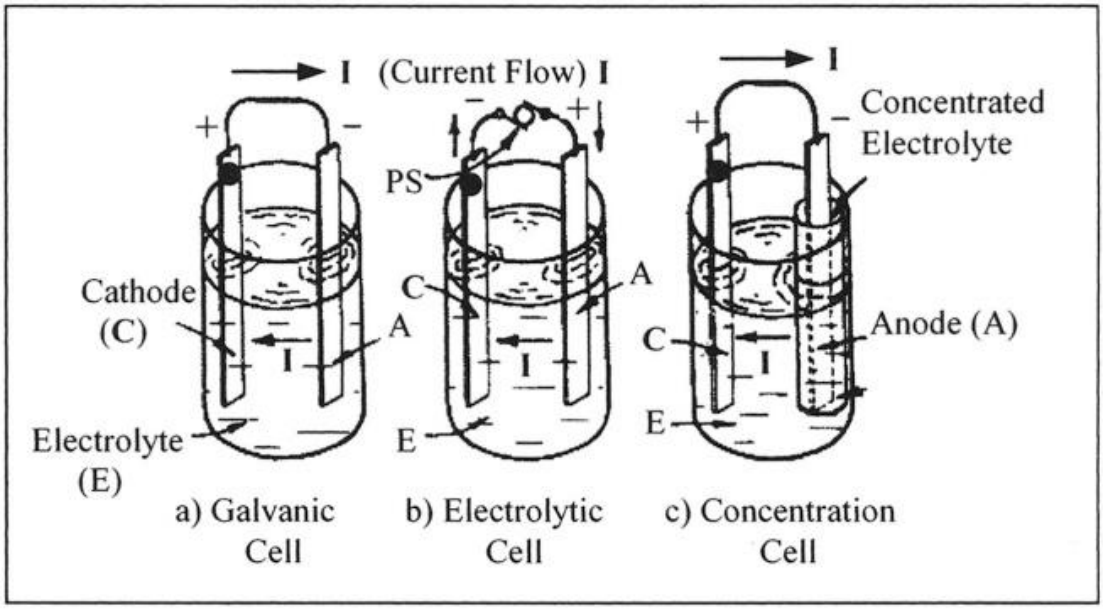

Figure 7: Types of Electrochemical Cells [18]

In general, there are four basic components for electrochemical cells:

- an anode electrode, which is a metal in contact with the electrolyte allowing anodic reactions to take place.
- a cathode electrode, where reduction of different species occurs.
- an electrolyte which is an electrical conductive fluid or most soil.
- a power supply which is connected to the anode and cathode electrodes, providing the potential to the electrochemical system for reduction reactions (electrolysis) or current through the anode to protect the cathode from corrosion.

These requirements are illustrated schematically in *Figure 8*.

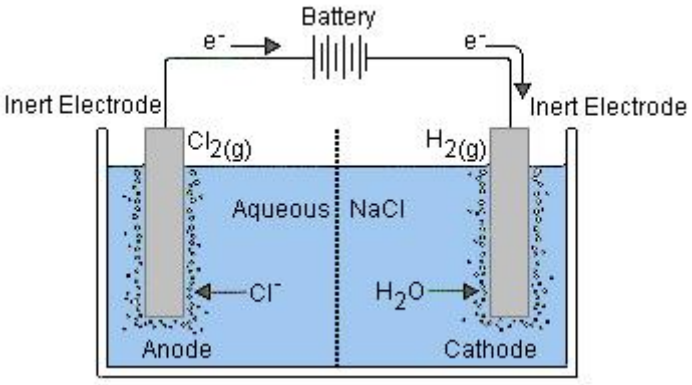

Figure 8: Schematic diagram of an electrolytic cell.

If an electrochemical cell produces energy, is known as a galvanic cell and if it consumes energy, as electrolytic cell. Nonetheless, an electrochemical process is treated as an electroanalytical technique associated with electricity and chemistry so that electrical quantities are measured in order to quantify chemical changes in a cell. Chemical measurements normally involve heterogeneous bulk solutions and electrochemical processes are analyzed according to the ionic interactions at the electrode-electrolyte interface.

3. KINETICS OF ACTIVATION POLARIZATION

3.1 Energy distribution [18][19]

Electrochemical reaction kinetics is essential in determining the rate of corrosion of a metal exposed to a corrosive electrolyte. On the other hand, thermodynamics predicts the possibility of corrosion, but it does not provide information on how slow or fast corrosion occurs. The kinetics of a reaction on an electrode surface depends on the electrode potential. Thus, a reaction rate strongly depends on the rate of electron flow to or from a metal-electrolyte interface. If the electrochemical system (electrode and electrolyte) is at equilibrium, the net rate of reaction is zero. In comparison, reaction rates are governed by chemical kinetics, while corrosion rates are primarily governed by electrochemical kinetics.

Electrochemical kinetics of a corroding metal can be characterized by determining at least three polarization parameters. These are corrosion current density (i_{corr}), corrosion potential (E_{corr}), and Tafel slopes $(\beta_\alpha$and/or$\beta_c)$. Then the corrosion behavior can be disclosed by a polarization curve (E *vs.* $\log i$). Evaluation of these parameters leads to the determination of the polarization resistance (R_p) and the corrosion rate as (i_{corr}), which is often converted into Faradaic corrosion rate C_R. This is an accelerated electrochemical process for determining C_R that has an advantage over the C_R determined by weight loss since the latter is a time consuming process, which may lead to unsatisfactory results when C_R changes with time. Instead, a polarization curve is readily obtained and it can offer a practical method for characterizing electrochemical kinetics parameters.

For a polarized electrode under steady-state current flow, the generalized reaction given by eq. $M = M^{+z} + ze^-$ can be used to derive the Butler-Volmer equation, which involves energy barriers known as activation energies. Only the activation energy change is used for the forward (ΔG_f) (reduction) and reverse (ΔG_r) (oxidation) reactions. For example, the hydrogen reaction, $2H^+ + 2e^- = H_2$ at equilibrium requires that the rate of discharge of H^+ ions in the forward direction (reduction) must be exactly equal to the rate of ionization of H_2 molecule in the reverse direction (oxidation). However, if deviation from the equilibrium state occurs, an overpotential develops and consequently, the electrochemical cell polarizes and the activation energies become dependent on the exchange current density(i_o). These energies are depicted in *Figure 9* in which the activation state is at

the maximum point (saddle point). This figure represents the Boltzmann or Maxwell Boltzmann distribution law for the energy distribution of the reacting species (ions).

This schematic energy distribution is for reversible electrodes. If these are polarized by an overpotential under steady-state conditions, the rates of reactions are not equal, $R_f \neq R_r$.

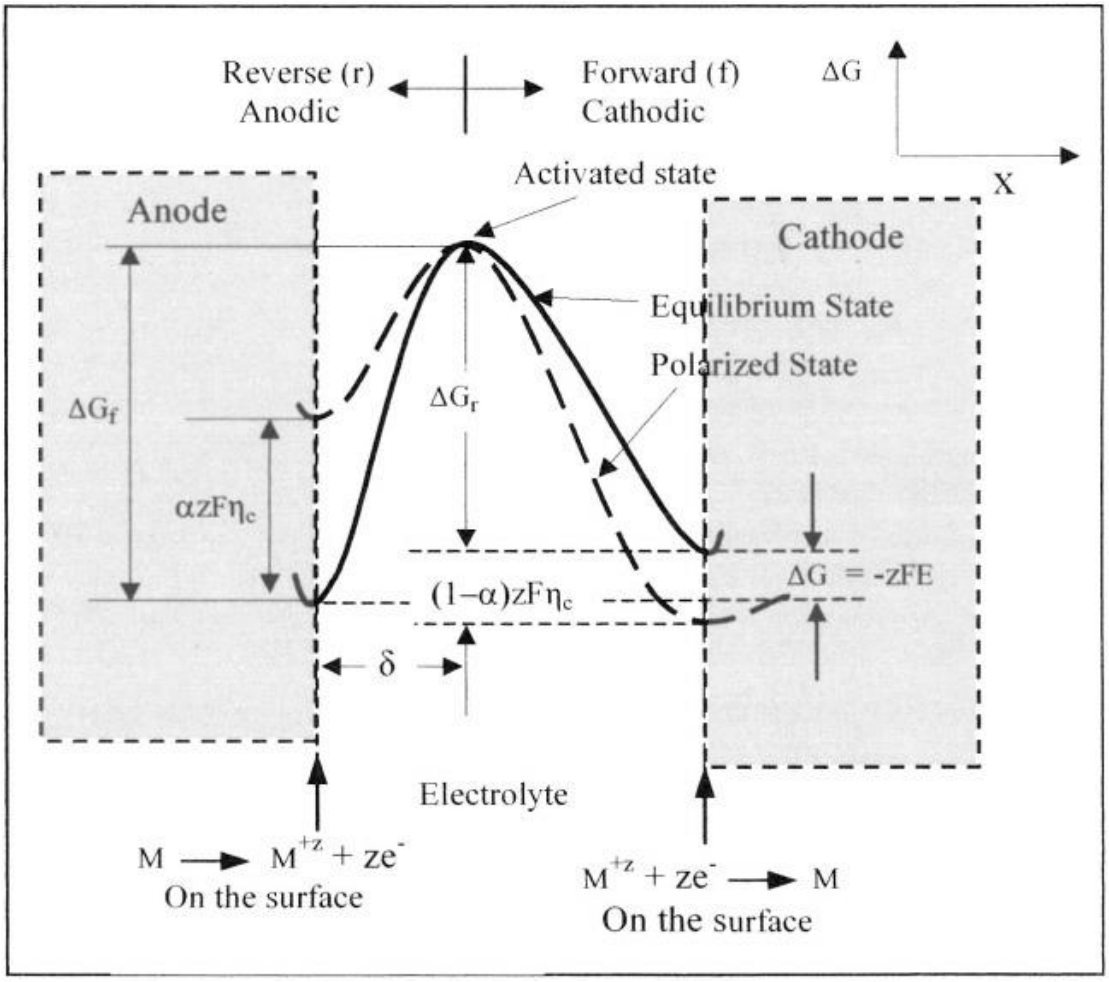

Figure 9: Schematic activation free energy distribution [18]

In general, the electrochemical and chemical rates of reactions due to either anodic or cathodic over potentials can be predicted using both Faraday and Arrhenius equations, respectively

$$R_F = \frac{iA_{\omega,j}}{zF} \qquad (3.1)$$

$$R_F = \gamma_\alpha \exp\left(-\frac{\Delta G^*}{RT}\right) \qquad (3.2)$$

At equilibrium, Faraday's and Arrhenius' rate equations become equal $R_F = R_A$ and consequently, the current density becomes:

$$i = \gamma_o \exp(-\frac{\Delta G^*}{RT}) \quad (3.3)$$

where, $\gamma_o = zF\gamma_\alpha / A_\omega$ may be defined as the electrochemical rate constant having unit of current density (A/cm^2). For a reversible electrode at equilibrium, the current density in eq. (3.3) becomes the exchange current density that is, i=i_o.

On the other hand, if an electrode is polarized by an overpotential under steady-state conditions, then the rates of reactions are not equal, namely ($R_F \neq R_A$) and consequently, the forward (cathodic) and reverse (anodic) current density components must be defined in terms of the free energy change ΔG^* deduced from Figure 9. Hence,

$$i_f = k_f' \exp\left[-\frac{\Delta G_f^*}{RT}\right] \text{(Cathodic)} \quad (3.4)$$

$$i_r = k_r' \exp\left[-\frac{\Delta G_r^*}{RT}\right] \text{(Anodic)} \quad (3.5)$$

Where, $\Delta G_f^* = \Delta G_f - \alpha zF\eta_c$

$\Delta G_r^* = \Delta G_r + (1-\alpha)zF\eta_\alpha$

α= Symmetry coefficient

For a cathodic case, the net current and the overpotential are $i = i_f - i_r$ and η_c respectively. Substituting eqs. (3.4) and (3.5) into this expression yields the net current density in a general form:

$$i = k_f' \exp\left(\frac{\Delta G_f}{RT}\right) \exp\left(\frac{\alpha zF\eta}{RT}\right) - k_r' \exp\left(\frac{\Delta G_r}{RT}\right) \exp\left[-\frac{(1-\alpha)zF\eta}{RT}\right] \quad (3.6)$$

from which the exchange current density is deduced as:

$$i_o = k_f' \exp\left(-\frac{\Delta G_f}{RT}\right) = k_r' \exp\left(-\frac{\Delta G_r}{RT}\right) \quad (3.7)$$

Substituting eq. (3.7) into (3.6) for one step reaction yields the well-known **Butler-Volmer equation** for polarizing an electrode from the open-circuit potential under steady-state conditions:

$$i = i_o\{\exp\left[\frac{\alpha zF\eta}{RT}\right]_f - \exp\left[-\frac{(1-\alpha)zF\eta}{RT}\right]_r\} \quad (3.8)$$

Where: η= E-E_O

E= Applied potential

It is clear that overpotential depends on the applied current density, therefore,$\eta = f(i)$. In addition, the exchange current density i_o can be defined as the rate of oxidation and reduction reactions at equilibrium. Specifically, i_o is the current density at which the rate of oxidation and rate of reduction are equal in a state of equilibrium. Thus, i_o is just the reversible reaction rate at equilibrium and it is a kinetic parameter, whereas ΔG is a thermodynamic parameter.

3.2 Electrochemical polarization [18][7]

Polarization (η) is the potential change, E-E_O, from the equilibrium half-cell electrode potential, E_O, due to the passage of an electrical current through an electrochemical cell causing a change in the working electrode potential. For cathodic polarization,η_c, electrons are supplied to the surface and a buildup in the metal due to the slow reaction rate causes the surface potential, E, to become negative to E_O. So, η_c is negative by definition. For anodic polarization, electrons are removed from the metal. This deficiency results in a positive potential change due to the slow liberation of electrons by the surface reaction, and η_a must be positive. Polarization is classified into two types: activation, concentration.

In this section is described the mathematical model which characterizes the kinetics of charge transfer mechanism involved in an electrochemical system. The figure below shows a partial polarization diagram and related kinetic parameters. Both Evans and Stern diagrams shows the significance of the electrochemical behavior of a polarized metal (*M*) electrode in a hydrogen-containing electrolyte.

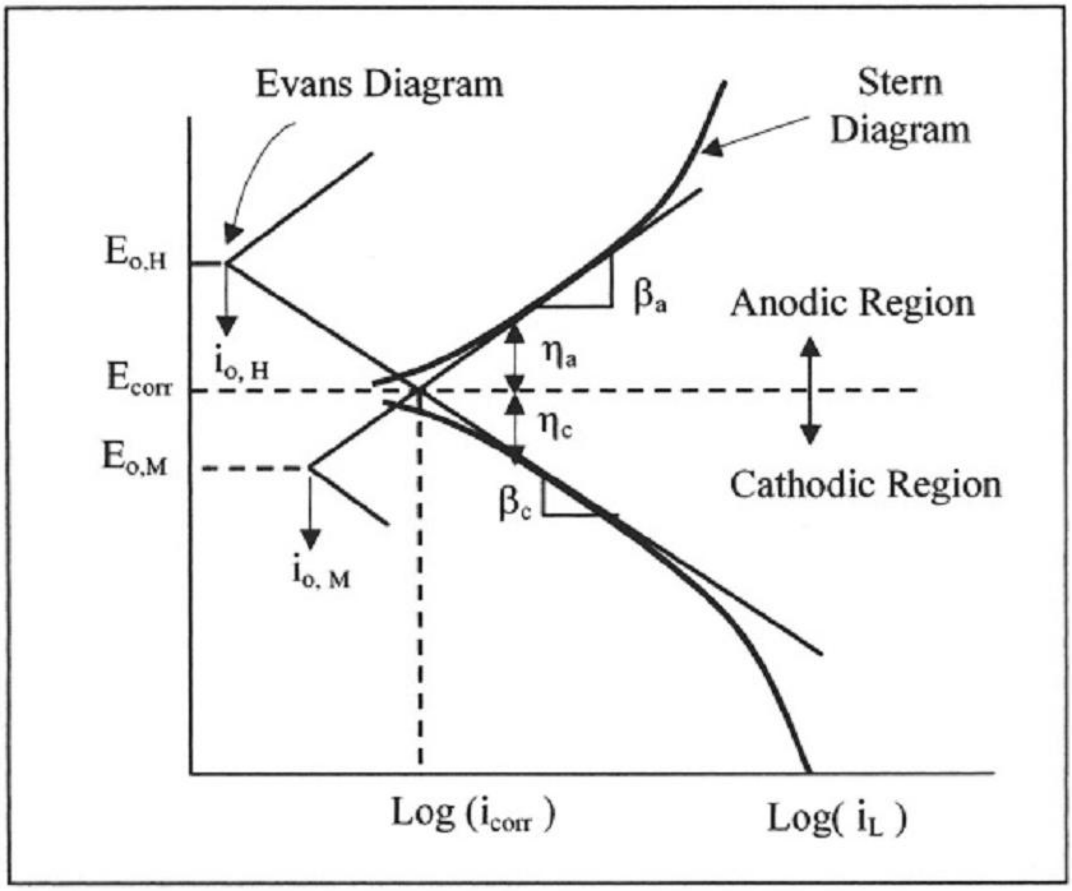

Figure 10: Schematic polarization curve showing Tafel extrapolation [18]

From *Figure 10*, $E_{o,H}$and$E_{o,M}$ are the open-circuit potentials for hydrogen and metal M, respectively, $i_{o,H}$and $i_{o,M}$are the exchange current densities, and i_L is the limiting current density.

For a reversible electrode, Evans diagram allows the determination of the corrosion point where both the hydrogen cathodic and the metal anodic line intercept. On the other hand, the irreversible electrochemical behavior denoted by the cathodic and anodic Stern diagram is also used for determining the corrosion point by simply extrapolating the linear portions of both curves until the intercept.

The *Figure 10*, is a very common in electrochemical studies of pure metals and their alloys. Therefore, both Evans and Stern polarization diagrams provide the corrosion potential (E_{corr})and the corrosion density (i_{corr}). Concerning the Stern diagram, this represents a polarization behavior that can be determined experimentally using potentiostatic and potentiodynamic methods, and it will be referred to as a polarization curve. Thus, a polarization curve is the result of polarizing from the

corrosion potential anodically or cathodically and it is a very common experimental output in electrochemical studies on corroding electrodes.

Evaluation of corrosion behavior is normally done through a function that depends on kinetic parameters depicted in *Figure 10*. Hence, the current density function for polarizing an electrode irreversibly from the corrosion potential is:

$$i = i_{corr}\{\exp\left[\frac{azF\eta}{RT}\right]_f - \exp\left[-\frac{(1-a)zF\eta}{RT}\right]_r\} \quad (3.9)$$

Anodic polarization caused by an anodic overpotential $\eta_\alpha = (E - E_{corr}) > 0$ is referred to as an electrochemical process in which a metal surface oxidizes (corrodes) by losing electrons. Consequently, the metal surface is positively charged due to the loss of electrons. This electrochemical polarization is quantified by η_α. On the other hand, cathodic polarization requires that electrons be supplied to the metal surface at an negative overpotential, $\eta_c = (E - E_{corr}) < 0$ which implies that E$< E_{corr}$.

3.2.1 Activation polarization [7][18]

In general, the activation polarization is basically an electrochemical phenomenon related to a charge-transfer mechanism, in which a particular reaction step controls the rate of electron flow from a metal surface undergoing oxidation. This is the case in which the rate of electron flow is controlled by the slowest step in the half-cell reactions.

Despite that eq. (3.1) is a generalized expression, it represents a measure of anodic polarization for corrosion studies and indicates that $\eta_a = 0$ for an unpolarized and $\eta_a \neq 0$ for a polarized electrode surface. For the latter case, the reaction rate for activation polarization depends on the charge-transfer over-potential as in metal oxidation due to electrons loss, the diffusion overpotential as in mass transport of ions, the reaction overpotential due to rate determining chemical reaction mechanism, the crystallization overpotential as in metal deposition in which atoms are incorporated into the electrode crystal surface lattice, and the Ohmic overpotential due to a resistance at the electrode/terminal junctions.

When some step in the half-cell reaction controls the rate of charge flow, the reaction is said to be under activation. Hydrogen evolution at a metal surface occurs, for example, in three major steps.

First, H^+ reacts with an electron from the metal,

$$H^+ + e^- \rightarrow H_{ads}$$

to from an absorbed hydrogen atom, H_{ads}, at the surface. Two of these absorbed atoms must react in the second step to form the hydrogen molecule

$$H_{ads} + H_{ads} \rightarrow H_2$$

A third step requires sufficient molecules to combine and nucleate a hydrogen bubble on the surface. Any one of the steps can control the rate of reaction

$2H^+ + 2e^- \rightarrow H_2$ and cause activation polarization.

The relationship between activation polarization, η, and the rate of the reaction represented by the current density,i_a or i_c is

$\eta_\alpha = \beta_\alpha \log\frac{i_a}{i_o}$ (3.10) for anodic polarization and

$\eta_c = \beta_c \log\frac{i_c}{i_o}$ (3.11) for cathodic polarization.

The Tafel relationships described by the previous equations have universally been observed by experiment for activation polarization. β_α& β_c are known as Tafel constants for the half-cell reaction.

For anodic overpotential, $\eta_\alpha$is positive and β_α must also be positive. Similarly, for cathodic polarization β_c is negative because η_c is negative.

The rate, as measured by i_a or i_c, increases by one order of magnitude for an overpotential change of +0.1V for anodic polarization and -0.1V for cathodic polarization, using the assumed values of β. The absolute values of β Tafel constants usually range from 0.03 to 0.2 and may not be equal for anodic and cathodic reactions. However +0.1 and -0.1V are reasonable estimates for β_α and β_c respectively for many purposes.

The theoretical derivation of the Tafel relationships is depicted in *Figure 11*.

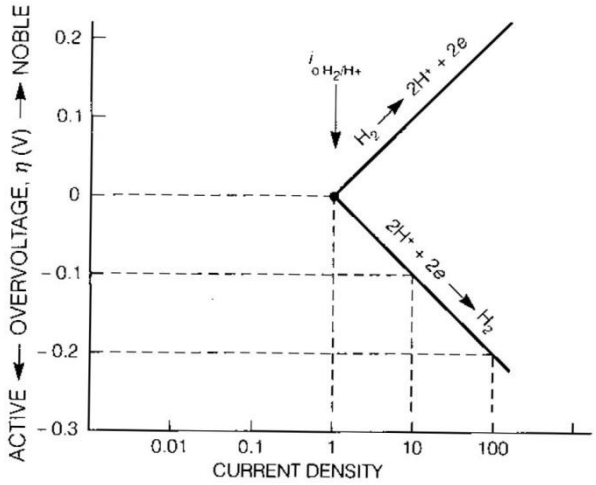

Figure 11: Activation overpotential showing Tafel behavior [7]

3.2.2 Concentration polarization

At high rates, cathodic reduction reactions deplete the adjacent solution of the dissolved species being reduced. The concentration profile of H^+ is shown in *Figure 12*. C_B is the H^+concentration of the uniform bulk solution and δ is the thickness of the concentration gradient in solution. The half-cell electrode potential e_{H^+/H_2} of the depleted surface is given by the Nernst equation as a function of H^+ concentration or activity H^+ ,

$$e_{H^+/H_2} = e^o_{H^+/H_2} + \frac{2.3RT}{nF}\log\frac{(H^+)^2}{P_{H_2}} \quad (3.12)$$

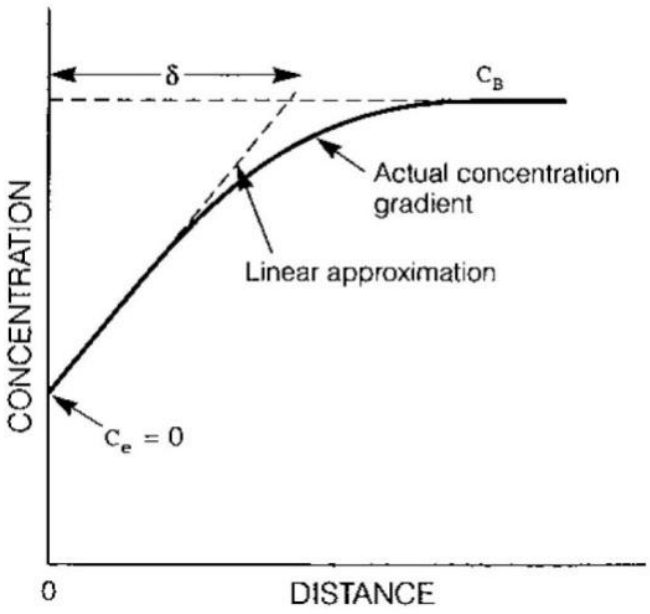

Figure 12: Concentration of H^+ in solution near a surface controlled by concentration polarization. [7]

3.2.3 Corrosion potential and current density

When a metal is corroding in an acid solution, both the anodic and cathodic half-cell reactions occur simultaneously on the surface. Each has its own half-cell electrode potential and exchange current density, as shown in *Figure 13*. However, the two half-cell electrode potentials cannot coexist separately on an electrically conductive surface. Each must polarize or change potential to a common intermediate value, E_{corr}, which is called the corrosion potential. E_{corr} is referred to as a mixed potential since it is a combination or mixture of the half-cell electrode potentials for the anodic and cathodic reactions.

Hydrogen is sometimes referred to as an oxidizer because it serves to 'oxidize' the metal to dissolved cations by its reduction in the cathodic reaction.

As reactions polarize on the same surface, the half-cell electrode potentials change respectively, according to

$$\eta_\alpha = \beta_\alpha \log \frac{i_a}{i_o} \quad \text{and} \quad \eta_c = \beta_c \log \frac{i_c}{i_o}$$

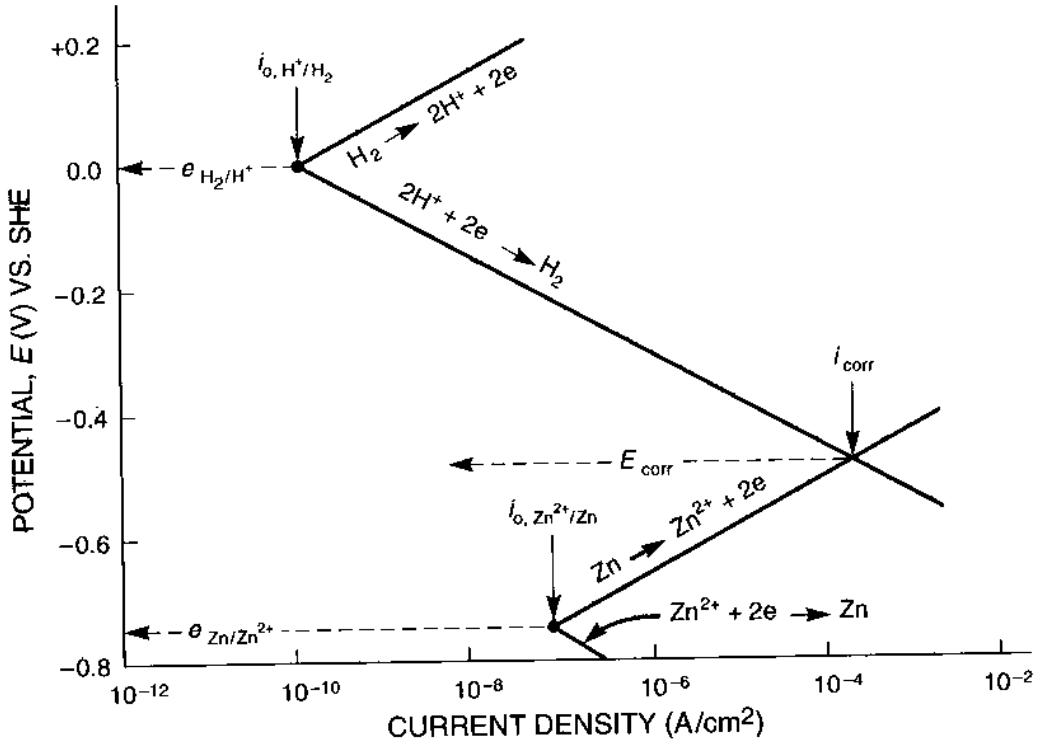

Figure 13: Anodic and Cathodic half cell reactions present simultaneously on corroding zinc surface. [7]

Until they become equal at E_{corr} as shown in *Figure 13*. The previous relationships for activation polarization are linear. The rate of anodic dissolution, i_a is identical to the corrosion rate i_{corr} in terms of current density and

$$i_c = i_a = i_{corr} \quad \text{at} \quad E_{corr}$$ as indicated in the previous figure.

3.3 POLARIZATION METHODS [18]

The polarization resistance R_p of a metal/electrolyte system and the pitting or breakdown potential E_b can be determined using at least two-electrode system. Subsequently, the rate of metal dissolution or corrosion rate is calculated using a function of the form $i_{corr} = f(\beta, R_p) > i_o$. The methods are:

- Linear Polarization (LP) as schematically shown in *Figure 14* covers both anodic and cathodic portions of the potential *E* versus current density i curve for determining R_p.
- Tafel Extrapolation technique (TE) (*Figure 15*) takes into account the linear parts of the anodic and cathodic curves for determining R_p.
- Electrochemical Impedance Spectroscopy (EIS) requires an alternating current (AC) and the output is a Nyquist plot for charge-transfer or diffusion control process.

In this thesis, the first two polarization methods have been used. Next sections describe Linear Polarization method and Tafel Extrapolation technique.

3.3.1 Linear Polarization

The linear polarization or Polarization resistance is confined to a small magnitude of the overpotentials η_α & η_c respectively, using linear coordinates. This technique allows the determination of i_{corr} using a potential range of ±10 mV from the E_{corr}. Before determing i_{corr} , the polarization resistance R_p is estimated from the linear slope of the curve as

$$R_p = \frac{\Delta E}{\Delta i} = \frac{\eta}{\Delta i} \quad (3.13)$$

$\frac{\Delta E}{\Delta i}$: the slope of the graph of Polarization Resistance. ΔE is in volts (V) and Δi is in (μA). The slope has units of resistance (polarization resistance).

The corresponding corrosion current density depends on kinetic parameters since $i_{corr} = f(\beta, R_p)$. Thus, the simple linear relation that defines the corrosion current density is of the form:

$$i_{corr} = \frac{\beta}{R_p} \text{ (3.14), where } \beta = \frac{\beta_\alpha \beta_c}{2.303(\beta_\alpha + \beta_c)}$$

Notice that equation 3.14 predicts that the corrosion current density is very sensitive to changes in the polarization resistance. In fact, the magnitude of the polarization resistance is mainly controlled by the corrosion current density.

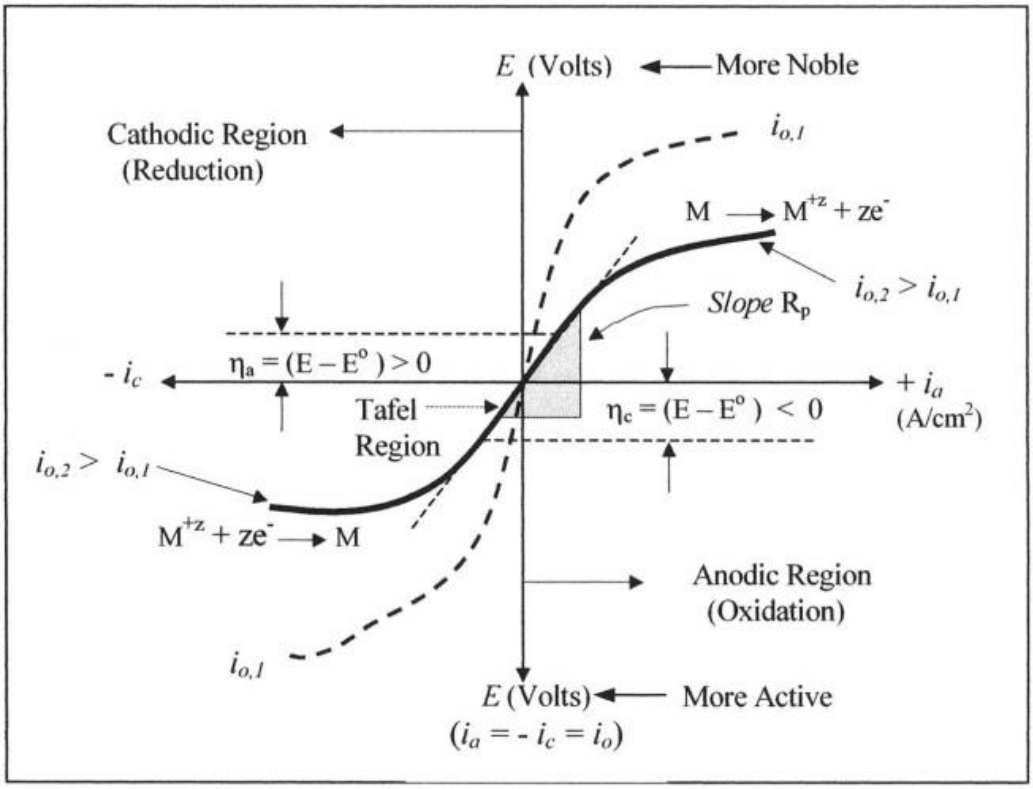

Figure 14*: Schematic linear polarization curve.* [18]

3.3.2 Tafel Extrapolation technique

This method involves the determination of the Tafel slopes β_α & β_c as well as E_{corr} and i_{corr} from the polarization curve as shown in *Figure 15*. This curve is known as the Stern diagram (non-linear polarization).

The corrosion current i_{corr} Tafel diagram taken from an extrapolation of the linear portion of the curve at value of the corrosion potential E_{corr}. The corrosion rate can be calculated from the value of i_{corr} by the following equation:

$$\text{Corrosion Rate (mpy)} = \frac{0.13 x i_{corr} x (E.W.)}{d} \quad (3.15)$$

The anodic and cathodic Tafel graphs described by the Tafel equation:

$$\eta = \beta \log \frac{i}{i_{corr}} \quad (3.16)$$

Where:

η : overpotential, the difference between the potential of the specimen and the corrosion potential (E_{corr}),

β : Tafel constant,

i_{corr}: corrosion current,

i: current in overpotentional η

From the previous equation, arises the following:

$$\eta = \beta \, (\log i - \log i_{corr}) \quad (3.17)$$

This equation has the form: y = mx + b, so a diagram of the overpotentional to logi is a straight line with slope β.

The Tafel constants β_α and β_c are calculated from the anodic and cathodic parts respectively of Tafel graph. Tafel constants, as mentioned above, are used for calculation of the corrosion rate of polarization resistance data.

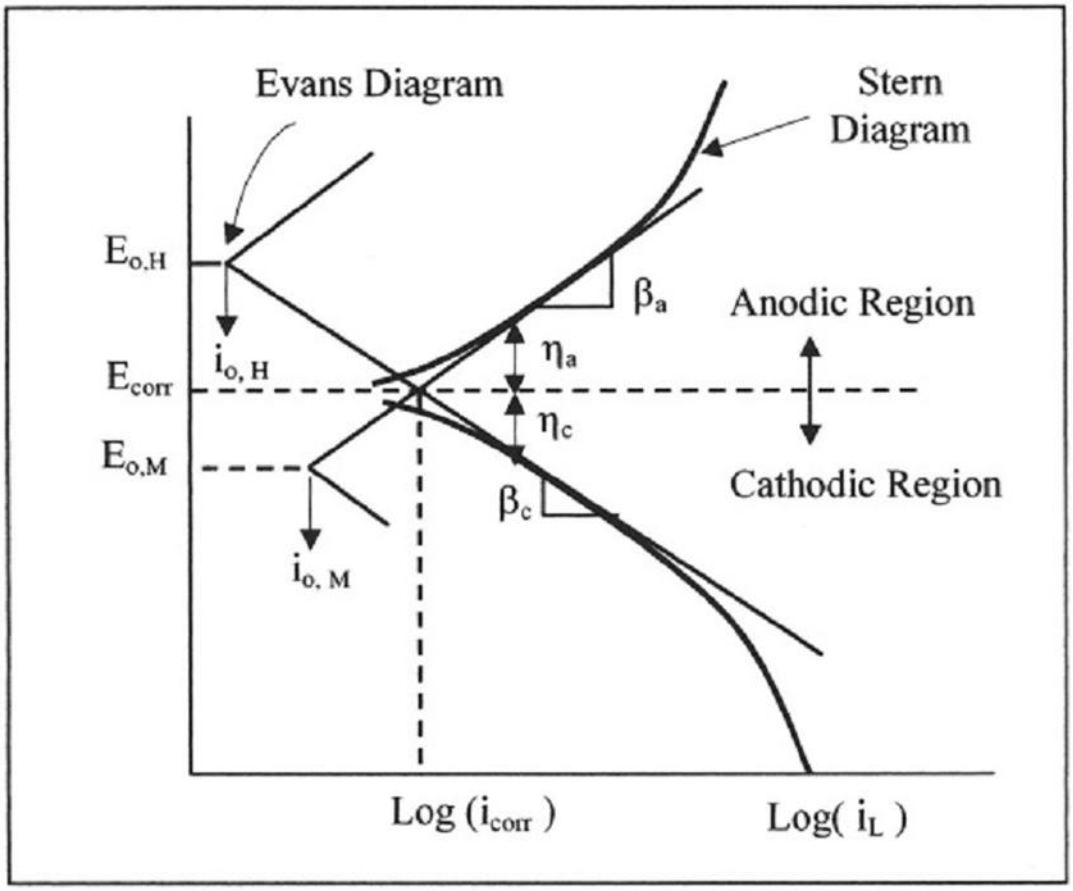

Figure 15: Schematic polarization curve showing Tafel extrapolarization. [18]

Tafel graphs provide a direct measurement of the corrosion current, which is related to the corrosion rate. This technique compared to the method of mass loss is extremely fast. The Tafel constants β_α and β_c, which are obtained, can be used in the method of Polarization Resistance to calculate the exact value of the corrosion rate.

4. STATE OF THE ART FOR CORROSION MODELLING

4.1 Introduction [12]

During the past 10 years, there has been an increased interest in modelling and simulation of material and process behavior in industry. In this chapter an attempt is made to summarize some application for modelling and simulation techniques to corrosion issues. It presents numerical models and simulation from the microscale to the macroscale for corrosion of aluminium (Al) alloys, typically used for aircraft constructions industry which is more developed than other industries. However, the approach is also applicable to a range of structures such as automotive and shipbuilding industry.

The use of numerical modelling and simulation methods is of high interest for materials and process development in the shipbuilding and aviation industry. In addition to helping achieve a better understanding of the behavior of materials, modelling and simulation also can help to reduce experimental testing time needed for development of new materials and processes. The greatest benefit obtained by sensible combination of numerical simulation and experimental investigation, while still taking into account the feedback data from the in-service experience to shipbuilding. In order to achieve accurate chemical, physical and numerical models, besides experimental validation of the model output, the quality of the input parameters are also essential factors for reliable numerical results.

Complex numerical models and simulations from the microscale to the macroscale have been developed for the corrosion of alloys. The main motivation for developing the corrosion models and simulation is to make significant technical advancements in the fields of naval design, surface protection systems against corrosion, and maintenance. The corrosion models that are developed in the literature, address pitting and intergranular corrosion (microscale) of alloys, crevice corrosion in occluded areas, such as joints (mesoscale), galvanic corrosion of structural elements (macroscale), as well as the effect of surface protection methods.

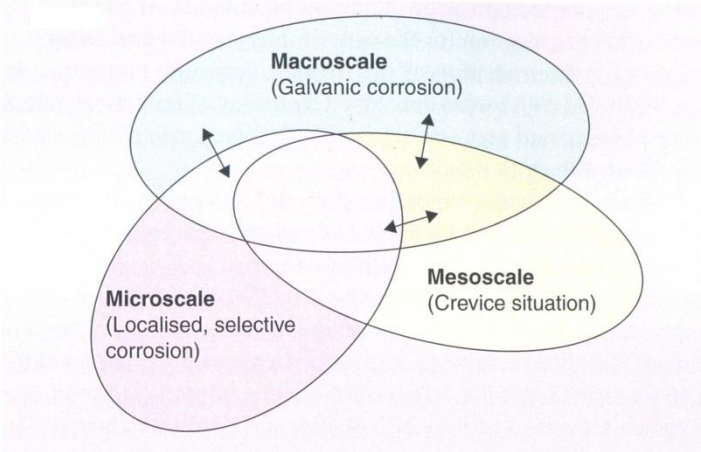

Figure 16: Schematic illustrating multi-scale modelling [12]

The simulation of electrochemical reactions at the microscale can be developed with a mechanistic, mass transport model (MTM) and a probabilistic, cellular automata model (CAM). The mass transport model is used to simulate local dissolution processes, such as those occurring during pitting and crevice corrosion. The cellular automata model simulates the corrosion propagation path for intergranular corrosion.

4.2 Microscale modelling [8][16]

4.2.1 Introduction

Microscale (pitting) corrosion of alloy can be modeled using a mass transport model (MTM), provided proper input data are supplied. Normally, such input data for the MTM are microstructural and localized (Microscale) corrosion properties of Al alloy.

MTM for simulation of localized corrosion events in aluminium alloys have been developed. This simulation is a multi-ion transport and reaction model (MITReM) which simulates micropolarisation curves measured over specific phases of Al 2024 alloy. However, the micropolarisation curve simulation excludes the pitting regime. The other MTM simulates localized corrosion within a deep, narrow crevice in Al 2024 in order to determinate the aggressiveness of local conditions at grain boundaries. The models predict the solution potential and the concentration profiles for all chemical species which appear either before (MITReM) or after (MTM) the onset of the localized corrosion process.

4.2.2 MITReM for localized corrosion

The mathematical model employed for simulation of localized corrosion consists of a steady-state balance equation for each species in the electrolyte solution:

$$-\vec{\nabla}\cdot\vec{\mathrm{N}}_i+\sum_{r=1}^{R}s_{ir}v_r=0 \quad (4.1)$$

Where N_i is the flux, v_r is the rate of reaction r and s_{ir} is the stoichiometric coefficient of species i in the reaction.

The flux of a species is caused by diffusion and migration:

$$\vec{N}_i=-D_i\vec{\nabla}c_i-\frac{z_iFD_i}{RT}c_i\vec{\nabla}U \quad (4.2)$$

Where D_i is the diffusion coefficient, F is the Faraday's constant, R is the universal gas constant, T is the temperature, and U is the local solution potential.

The convective transport is omitted because the electrolyte solution near the surface is stagnant. The electrolyte solution is electrically neutral at the local scale:

$\sum_{i=1}^{I} z_i c_i = 0$ (4.3), where c_i is the concentration and z_i is the charge number of species i.

Beyond the diffusion layer near the Al 2024 solution interface, bulk concentrations of chemical species prevail. Therefore, bulk concentrations are imposed on the top boundary of the diffusion layer.

As Ohms law is valid outside the diffusion layer and the counter electrode is positioned far away from the Al 2024 surface, the top boundary of the diffusion layer will be approximately an equipotential plane. This fact allows a reference potential, U=0, to be imposed at this boundary.

The purpose of the MITReM model is to attempt to better understand the onset of localized corrosion by taking into account the difference in reaction kinetic rates, while the MTM model was developed in order to model the aggressiveness of local conditions at grain boundaries and determinate the risk of transition from localised corrosion to macroscopic propagation of corrosion, for example, intergranular corrosion.

MITReM has been exploited to make a three-dimensional model of the microscale galvanic interaction. The model outputs results are predicted values and distributions for the electrochemical potential and species in the electrolyte solution and simulation of polarization curves measured over an area of Al 2024 which contains a specific distribution of particles.

MTM was developed using the software Comsol and can model changes in local electrolyte composition as a function of the microscale geometry and cathodic sites within the Al 2024 and imposed dissolution rates which are representative for pitting conditions. The model includes metallic ionic species resulting from electrochemical reactions at the metal-solution interface and reactions in solution and assumes one anodic site at the crevice bottom and cathodic site both on the Al 2024 surface and in the crevice. It is shown that attack propagation requires electrical coupling between the anodic site and cathodic site on the sample surface, resulting in high dissolution rates. If only the cathode is active, the attack will propagate with slower rates, depending on the crevice depth due to oxygen depletion in the crevice.

Considering the very high complexity of aluminium alloys containing multiple phases, the results obtained are in very good agreement with the experimental measurements.

4.3 Macroscale modelling [21]

4.3.1 Introduction

In this chapter, the critical parameters that dominate the galvanic corrosion will be analyzed. A mechanistically based computational model will be described and validated by comparison with experimental results.

4.3.2 Galvanic Corrosion Model

The boundary element method (BEM) has been frequently used to model Galvanic Corrosion as it has many advantages for this type of application.

The mathematical description of the problem is based on 3-D Poisson equation for the electrolyte potential with non-linear boundary conditions imposed by the prescribed polarization curves on the active electrodes. The physical and mathematical background for the modeling apart from the following equations:

$$cV_e(x) + \int_\Gamma \frac{\partial G(x,y)}{\partial n} V_e(y) d\Gamma(y) - \int_\Gamma G(x,y) \frac{\partial V_e(y)}{\partial n} d\Gamma(y) = 0 \quad (4.4)$$

The previous equation describes the potential at any point x in terms of sources distributed on the boundary Γon the integration domain.

$G(x,y)$ is the Green's function of Laplace equation, x,y ∈ R^3 are vectors in 3-D space, n is the outward unitary normal of the boundary of the integration domain and c is a constant whose value is 0 if x is outside the integration domain,1 if interior and a value $0 < c < 1$, which depends on the local curvature of the boundary if x∈ Γ.

Then, boundary discretization is applied and a collocation technique is used to represent potentials and normal current densities on each boundary element in terms of M interpolating functions W(η_1,η_2). In this way, eq. (4.4) yields

$$cV_e(x)+\sum_{j=1}^{N}\sum_{k-1}^{M}H_{jk}V_{kj}-\sum_{j=1}^{N}\sum_{k=1}^{M}G_{jk}\frac{\partial V_{kj}}{\partial n}=0 \quad (4.5)$$

$$\text{Where } G_{jk}=\int_{\Gamma_1}G(x,\vec{\eta})W_k(\vec{\eta})d\Gamma_j \;\&\; H_{jk}=\int_{\Gamma_1}\frac{\partial G(x,\vec{\eta})}{\partial n}W_k(\vec{\eta})d\Gamma_j \quad (4.6)$$

represents the integrals of the single and double layer potentials, respectively, $\vec{\eta}=(\eta_{1,}\eta_2)$ represent the local coordinates of the element and $d\Gamma_j$ is the differential surface area of the integration. Potentials and normal current densities on the *j*th boundary element are represented in terms of the interpolating functions and their nodal values as

$$V_e(y)+\sum_{k=1}^{M}W_k(\eta_1,\eta_2)V_{kj} \quad \& \quad \sigma\frac{\partial V_e(y)}{\partial n}=\sigma\sum_{k=1}^{M}W_k(\eta_1,\eta_2)\frac{\partial V_{kj}}{\partial n}\text{, respectively.}$$

Equation (4) leads to an algebraic systems of equations, in which unknown are potentials and current densities normal to the boundary evaluated on the boundaries of the electrolyte. The eq. (3) and (4) involve only the boundary of the integration domain.

This model developed using the finite element method (FEM) to model the thin films and BEM for the deeper or bulk electrolyte situations. The model consists of two co-planar electrodes immersed in an electrolyte.

The outcomes of the simulation are essentially the potential distribution and the three-dimensional components of the current density anywhere on the model, as well as its integral over selected surfaces, that is, total flowing to each electrode.

4.4 Mesoscale modelling [23]

4.4.1 Introduction

The modelling approach in this section is based on crevice models. The simulations were performed at the mesoscale (millimetric range) using finite element analysis (FEM). Crevice corrosion is initiated by changes in the local chemistry within the crevice which lead, in most cases to acidic pH.

A mass transport and reaction model was applied to understand and quantify the possible chemical and electrochemical changes that occur in an occluded cell in relation to the lab joint design. The purpose is to model the electrochemical and chemical evolution leading to localized corrosion inside a narrow gap containing electrolyte which can be encountered within a sensitive lap joint in some parts of an aircraft as a function of the relevant physical parameters.

4.4.2 Simulation approach

Using Comsol Multiphysics software to solve the basic differential equations (Nernst-Planck equation) describing the mass transfer, the electrochemical and chemical reactions occurring inside the cavity, simulations were performed to calculate the chemical changes inside an aluminium crevice. The model solved for both the steady and time-dependent states using finite element method (FEM) analysis.

In the electrolyte, the motion of the species follows the Nernst-Planck equation at steady state:

$$\frac{\partial C_i}{\partial t} = R_i - \nabla N = 0 \qquad (4.7)$$

The flux density for each species, i, in the electrolyte is given as follows:

$$N = -D_i \nabla C_i - z_i u_i F C_i \nabla V \quad (4.8)$$

Equation 4.8 results from the summation of diffusion term and an electro-migration term. C_i and z_i are the values of concentration and charge for species i respectively. F is the Faraday constant and V is the electrostatic potential in the solution. The experimental measurements and the simulated results are in very good agreement.

4.5 Atomistic-nano modeling [2][10]

Atomistic modeling techniques can be grouped into four main categories:

- Molecular modeling encompasses the field of (generally) small-molecule calculations.
- Static band-structure calculations, is used to solve the electronic structure problem, which in turn allows access to molecular properties,
- Molecular dynamics can be used to simulate reaction events, particularly those involving high energy or thermally stimulated processes.
- Monte Carlo simulations go beyond dynamic effects but utilize atomistically determined information for the rate constants of fundamental atomistic and molecular transformations to perform stochastic updates to the state of a system, which, in this context, may be considered its atomistic configuration.

Combined atomistic and continuum simulation plays an important role in nanomechanics because of three reasons:

- Multiscale failure behaviors,
- Ever-limited computational resources even though they are much powerful than before
- Insufficient experimental information at the atomistic scale.

Continuum theory by itself is insufficient to explain nanoscale observations. Materials have atomistic scale structures that affect their macroscopic behavior. Though it is fundamental, atomistic vision of material behavior is limited by the computational possibilities.

Fracture apart from phenomena occurring at a range of length scales. While a crack propagates in the macroscopic scale, the crack tip always involves atomic scale behavior of successive atomic debonding. With modern computers the atomistic simulation tends to larger scale and continuum simulation goes to smaller scale. Continuum method is excellent in describing the large field. However, the approach generally represents an averaged characteristic. It gives an incomplete prediction of the local state of a nanoscale structure. Studies at the atomistic level are needed to understand the exact nature of the crack-tip responses. The requirement is a proper description of the interatomic potential.

Molecular Dynamics (MD) simulates physical movements of atoms and molecules. The atoms and molecules are allowed to interact for a period of time, giving a view of the motion of the atoms. In the most common version, the trajectories of atoms and molecules are determined by numerically solving the Newton's equations of motion for a system of interacting particles, where forces between the particles and potential energy are defined by interatomic potentials or molecular mechanics force fields. The method was originally conceived within theoretical physics in the late 1950s but is applied today mostly in chemical physics, materials science and the modeling of biomolecules.

The important difference between continuum and MD models is the role of inertia, which dominates in the atomistic models. The transition from a stationary to a moving crack, as a function of the applied driving force, occurs continuously in continuum models. However, in atomistic models with strong-ranged bonds the transition is discontinuous and exhibits hysteresis as a function of the driving force. The absence of atomic inertia effects in continuum models cause this difference.

4.6 Multiscale Modelling [10]

Material failure is a process with information at several scales. The geometric complexity is complicated further by the interactions among structural features at different scales. In addition to the structural hierarchy of polycrystalline materials it is essential to recognize their dynamical nature. Processes at various length scales usually possess different relaxation times, suggesting that in addition to the spatial hierarchy a temporal one exists. Microstructures are only a reflection of the fact that a polycrystalline material has not had enough time to reach equilibrium. Also, microstructures are path and history dependent, adding further complexity to understanding and controlling their evolution. Combined atomistic and continuum simulation provide a basic tool in understanding multiscale material behaviors. The main idea in the coupled atomistic and continuum approach is to use atomistic modeling at places where the variation is on an atomic scale, and the continuum approach elsewhere. The challenging problem comes with the communication between two descriptions of the materials.

4.6.1 Lattice Green's Function

Lattice Green's function calculates the static structure of defects in a lattice. In this approach, the actual number of atomic degrees of freedom is not changed, but rather a large proportion of the atoms are treated using a linear approximation to their response. These linear atoms, while they are still explicitly modeled, demand considerably less computational overhead than fully nonlinear atoms. Thus, this approach greatly reduces the calculation time.

4.6.2 Quasicontiniuum Method

QC method is used for multiscale simulations. The QC theory starts from an underlying conventional atomistic model and strives to systematically eliminate redundant degrees of freedom. In this method, interatomic interactions are incorporated in the model via the discrete lattice calculation based on the local state of deformation. The QC method links atomistic and continuum models through the device of the FE method that permits a reduction of the full set of atomistic degrees of freedom. The QC method differs from FEM in that the constitutive input is drawn directly from calculations at the atomic scale.

Both lattice Green's function and QC methods are static methods. These methods are effective in seeking long-term balanced configurations, and time scale is not a difficult issue in these approaches

4.7 Density Functional Theory [14]

Density-functional theory is one of the most popular and successful quantum mechanical approaches to matter. Density Functional Theory (DFT) is a ground-state theory in which the emphasis is on the charge density as the relevant physical quantity. DFT has proved to be highly successful in describing structural and electronic properties in a vast class of materials, ranging from atoms and molecules to simple crystals to complex extended systems (including glasses and liquids). Furthermore DFT is computationally very simple. For these reasons DFT has become a common tool in first-principles calculations aimed at describing – or even predicting – properties of molecular and condensed matter systems.

To get a first idea of what density-functional theory is about, it is useful to take a step back and recall some elementary quantum mechanics. In quantum mechanics, all information we can possibly have about a given system is contained in the system's wave function, Ψ. Here we will exclusively be concerned with the electronic structure of atoms, molecules and solids. The nuclear degrees of freedom (e.g., the crystal lattice in a solid) appear only in the form of a potential u(r) acting on the electrons, so that the wave function depends only on the electronic coordinates. Non-relativistically, this wave function is calculated from Schrödinger's equation (4.9), which for a single electron moving in a potential u(r) reads:

$$\left[-\frac{h^2\nabla^2}{2m}+u(r)\right]\Psi(r)=\varepsilon\Psi(r) \quad (4.9)$$

If there is more than one electron Schrödinger's equation becomes:

$$\left[\sum_i^N(-\frac{h^2\nabla^2}{2m}+u(r_i)+\sum_{i<j}U(r_i,r_j)\right]\Psi\,(r_1,r_2\dots,r_N)=E\Psi(r_1,r_2\dots,r_N) \quad (4.10)$$

Where N is the number of electrons and $U(r_i,r_j)$ is the electron-electron interaction.

5. EXPERIMENTAL INVESTIGATION

5.1 Introduction

The following sections describe the experimental procedure that had been followed step by step, as well as the principles of experimental methods.

5.2 Processing

5.2.1 Cutting off Process

The first step was the cutting. The purpose of cutting is to section a representative, yet manageable sample from a large or irregular piece of a given material, or to obtain sections in specific angles, for example cross sections. The bars were cut in sections using the Struers Discotom 50 *(Figure 17).* For each electrochemical test, specimens of 20mm x plate thickness 12mm were cut.

Figure 17: Discotom. of Naval Technology Lab.

5.2.2 Cold Mounting Process

After finishing with the cutting off process, coming up next was the cold mounting process. Each specimen was mounted to epoxy resin. Mounting allows for a safer, more convenient handling of small, sharp or irregularly shaped specimens or when the protection of layers is imperative. Cold mounting is especially suited for mounting specimens that are sensitive to heat or pressure. Additionally, cold mounting does not require an investment in a mounting press and is therefore good for infrequent mounting tasks. The resin, a mixture of two or three components, is poured over the specimen after it has been placed in a mounting cup. After curing for 24 hours, the specimen can be taken out of the cup and processed. Samples were mounted using the EpoFix Kit (*Figure 18*) from Struers before experiment, leaving an exposed area of 20 mm × 12 mm on the material surface.

Figure 18: Specimens immersed with an epoxy resin

5.2.3 Grinding Process

Grinding is the next stage in mechanical material removal. Proper grinding removes damaged or deformed surface material while introducing as little new deformation as possible, thus preparing the sample surface for polishing if necessary. The back side of the specimen was free of epoxy resin. Grinding is divided into two processes: Plane Grinding and Fine Grinding.

Plane Grinding

The grinding process always begins with plane grinding. Plane grinding ensures that the surfaces of all specimens are in the same condition before the preparation continues, and that the surfaces of all specimens in a specimen holder are at exactly the same level.

Fine Grinding

Fine grinding must remove the deformation existing from cutting or plane grinding and produce a surface that is ready for experimentation. Choosing the correct fine grinding materials is vitally important to ensure fast and economical preparation. The equipment we use for the process was:

- Struers LaboPol – 5 (*Figure 19*)
- Struers MD-Fuga Silicon Carbide Papers: 80 grade - 180 grade - 320 grade – 800 grade – 1000 grade - 1200 grade – 1500 grade.

Figure 19: Struers Laboforce-5

5.3 Electrochemical measurements

For our electrochemical measurements we used a three electrode cell to investigate the corrosion properties of the specimens and calculate the corrosion rate.The apparatus employed (*Figure 20*), has the following characteristics:

- Electrolytic cell, K0235 Flat Cell - EG&G Princeton Applied Research-Perkin Elmer Instruments, *Figure 21*
- Saturated Calomel Electrode as reference electrode,
- Potentiostat-Galvanostat, VersaStatTM II of EG&G Princeton Applied Research-Perkin Elmer Instruments,
- 3.5% NaCl aerated solution (electrolyte), to simulate the seawater environment.

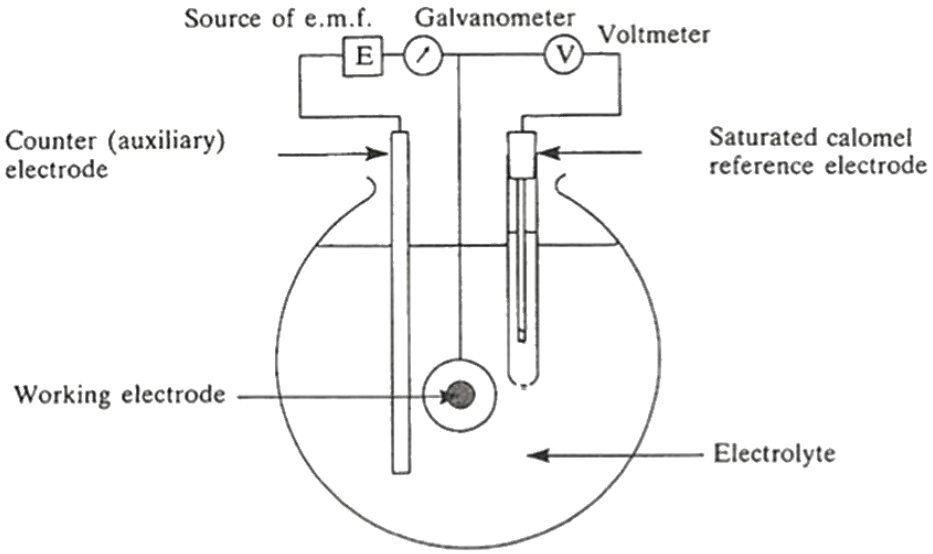

Figure 20: The experimental apparatus for the determination of polarization curves of a metal in a solution.

In order to evaluate the corrosion behavior of the specimens, Tafel polarization curves was employed, resulted from DC Large signal polarization. A Tafel graph is generated by the polarization of a metal specimen for about ±250 mV anodic (positive) and cathodic (negative), relative to the equilibrium potential (E_{eq}).

Next paragraphs describe the characteristics of the experimental equipment which used in order to take the measurements.

5.3.1. Electrolytic cell

The three-electrode cell, *Figure 21,* is the standard laboratory apparatus for the quantitative investigation of the corrosion properties of materials. It can be used in many different types of corrosion experiments. For the electrochemical measurements is used the three-electrode cell of the lab, K0235 Flat Cell. Below is a more detailed examination of its components.

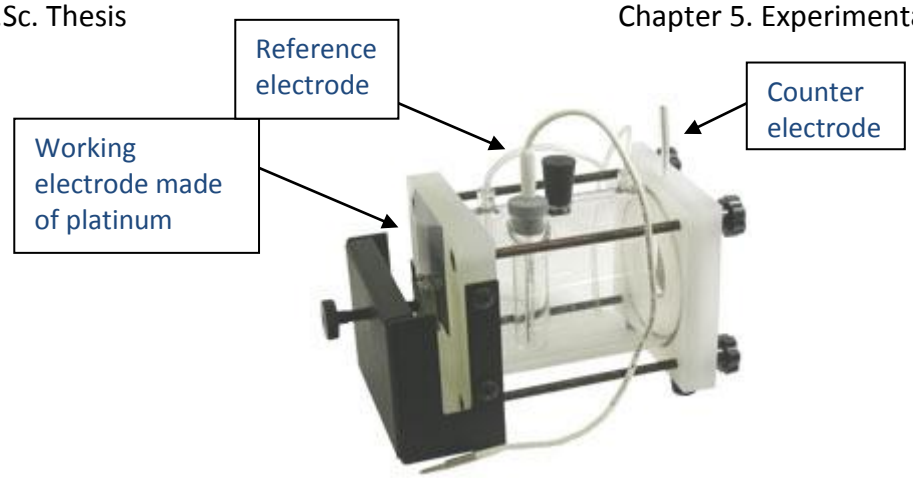

Figure 21: Electrolytic cell, K0235 Flat Cell

The working electrode

The working electrode is the name given to the electrode being investigated (AH36 and S690 steel). We use the term “working electrode” rather than “anode” because we are not limited to investigations of anodic behaviour alone, cathodic behaviour can also be examined. Electrical connection must be made to the specimen, and this can be done with solder or spot weld on the reverse side before mounting.

The counter electrode

The counter (auxiliary) electrode is the name given to the second electrode. The counter electrode is present specifically to carry the current created in the circuit by the investigation, it is not required for measurements of potential. Usually, a carbon rod is used, but it can be any material that will not introduce contaminating ions into the electrolyte. Platinum or gold can also be used with success, especially if space is at a premium, when smaller electrodes can be used, titanium is also suitable. In this experimental procedure the counter electrode is made of platinum.

The reference electrode

The reference electrode is present to provide a very stable datum against which the potential of the working electrode can be measured. The most convenient reference electrode to use in such an experiment is a saturated calomel electrode (SCE) which potential is E = +240mV vs. SHE. The electrode consists of a mercury reservoir covered with a paste of mercury - mercury chloride (calomel) immersed in potassium chloride. The contact is made with platinum wire immersed in mercury.

5.3.2 The Source of Potential

The relative potential - current of the working electrode, with the potentiostatic method, is determined by applying constant potential between the working electrode and the counter electrode. This is done by altering the current at the counter electrode to maintain the set value of working-to-reference potential. For the experimental procedure is used Potentiostat, VersaStatTM (*Figure 22*).

Figure 22: Potentiostat, VersaSTaT 4

5.3.3 The electrolyte

Electrolyte is a fundamental part of the whole corrosion process. It is extremely important to consider the conductivity of the electrolyte, since by carrying the ionic current, it plays very important role in corrosion reactions. The use of a reference electrode is to enable the potential of a working electrode to be measured and it should be placed as close to the electrode surface as possible. This is because the measured potential will always include the potential difference across the electrolyte occupying the space between the working electrode surface and the reference electrode. The solution used in the experiments is sodium chloride (NaCl) 3.5% w/w. According to the literature the value of the conductivity of this electrolyte is σ=500 S/m.

5.4 Results and Conclusions

The above mentioned electrochemical techniques were also performed for both metals AH36, S690.

From the electrochemical experiments performed, in the following paragraphs are presented the Tafel Polarization curves (mV/μA), resulted from DC Large signal polarization, for about ±250 mV anodic (positive) and cathodic (negative) relative to the equilibrium potential (E_{eq}), which are considered as the most representative for the corrosion evaluation.

5.4.1 Results of electrochemical experiments for metals: AH36, S690

In *Figure 23* the Potentiodynamic Tafel Curves are presented. The Tafel curves for metals present a slight difference in the corrosion potential E_{eq}, lower for AH36, thus from thermodynamic point of view, AH36 is more active to corrosion. However the values for the corrosion current i_{corr}, is rather similar, implying that the corrosion rate is similar for the two different metals.

Moreover the shape of the cathodic part of the curve shows that the phenomenon is controlled by the reduction of oxygen, in the solution:

$$O_2 + 2H_2O + 4e^- \rightarrow 4OH^-$$

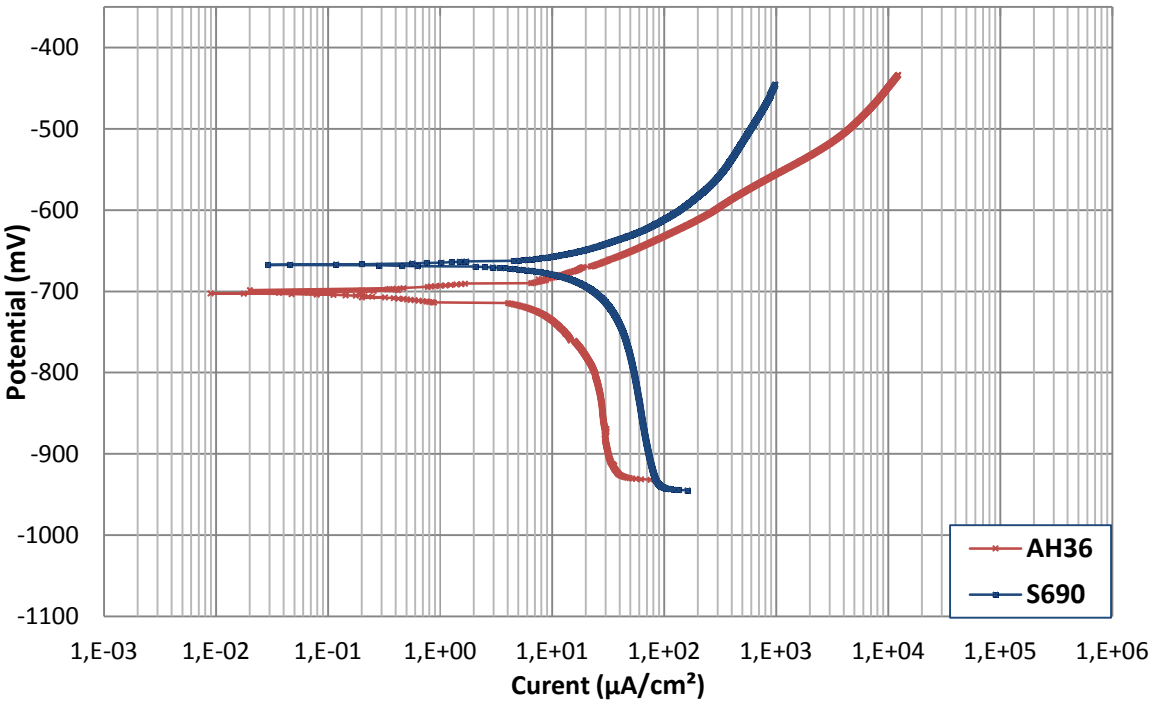

Figure 23: Comparison between AH36 and S690 Metals

However, no significant differences are observed for the corrosion rate in the electrochemical testing, showing that the phenomenon is mainly controlled by the oxygen reduction in the solution.

6. MODEL SET UP – COMSOL MULTIPHYSICS 4.3b [3][4][5][6]

6.1 Introduction

Computer simulation has become an essential part of science and engineering. Comsol Multiphysics is a commercial finite element package designed to address a wide range of physical phenomena. These phenomena are normally described mathematically using partial differential equations (PDE). Therefore, electrochemical experiments can be developed by solving such PDEs on a suitable geometry and timescale.

Comsol Multiphysics is designed for "multiphysics", namely, for incorporation and coupling of diverse physical phenomena, expressed as PDEs, within one model. The desired phenomena often originate from traditionally separate fields of applied physics and engineering. One electrochemical example of a "multiphysics" problem would be fuel cell analysis, which combines fluid dynamics, mass transport, heat transfer, and charge transfer. Multiphysics simulation can maximize physical insight and predictive power by describing accurately all relevant phenomena.

So as to develop a model with Comsol, it is necessary to define the space dimension, physics, and study method from the Model Wizard (*Figure 24*). The physics user interfaces contain predefined physics descriptions and equations for a variety of engineering and scientific disciplines.

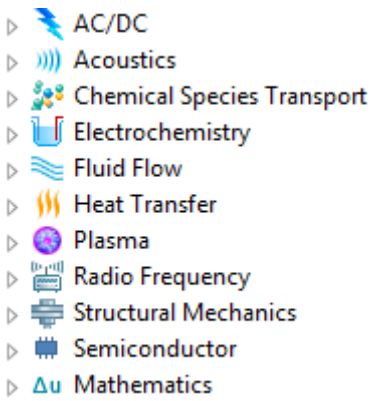

Figure 24: The physics list as shown in the Model Wizard.

6.2 Corrosion module

The Corrosion Module is intended for the modelling and simulation of corrosion and corrosion protection of metal structures subjected to aqueous electrolytes. The descriptions made available by this module are based on current and potential distribution in electrochemical cells.

The module defines models in 1D, 2D, and 3D that describe chemical species transport, fluid flow, heat transfer, electrochemistry, and corrosion interfaces. These physics interfaces describe the potential in the electrolyte and in the corroding or protected metallic structure. The electrode reactions can be described using arbitrary electrode kinetic expressions of the overpotential for the anodic and cathodic reactions. The simulations can be used to understand and avoid corrosion as well as to design and optimize corrosion protection.

The descriptions in the module allow for the simulation of systems at different scales and at different levels of detail. A model may include a set of geometrically complex structures with several hundred sacrificial anodes protecting the structure. The modeling and simulation capabilities of the Corrosion Module cover processes such as galvanic, pitting, and crevice corrosion. The capabilities also include, for example, systems for cathodic protection, sacrificial anode protection, and anodic protection.

6.3 Electrochemistry branch

The electrochemistry module is used in order to model the electrochemical experimental procedure in the present thesis. *Figure 25* depicts the interfaces which are found under the Electrochemistry branch in the Model Wizard.

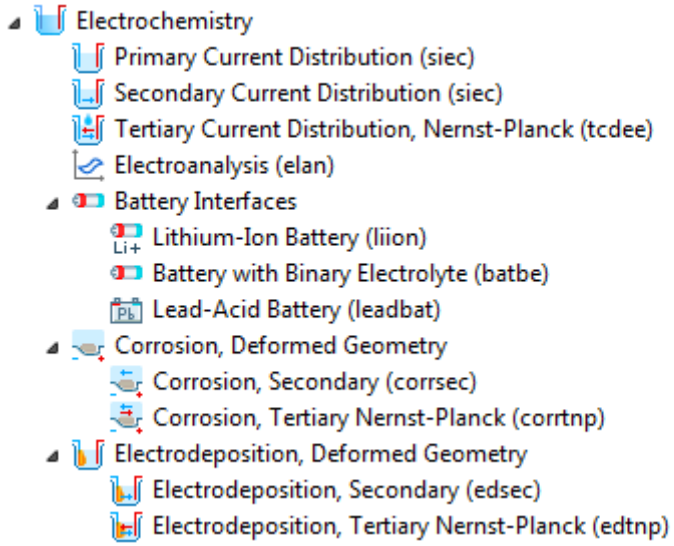

Figure 25: The interfaces are found under the electrochemistry module.

The Electrochemistry Module extends the Comsol Multiphysics environment with customized physics interfaces for modelling of electrochemical cells, with tools for building detailed models of the configuration of electrodes and electrolyte. The physics interfaces include descriptions of the electrochemical reactions and the transport properties that influence the behavior of various types of electrochemical cells. By this module it is possible to investigate the influence of using different materials, geometric configurations, and operating conditions on the behavior of a cell.

Some applications for this module are the following:

- Electroanalysis
- Rotating disc electrodes
- Voltammetry
- Chronoamperometry
- Electrochemical impedance spectroscopy
- Electrochemical sensors
- Electrolysis

- Electrodialysis
- Biosensors
- Electrochemical nanotechnology

In the model developed in this thesis, Secondary Current Distribution has been selected as solution method. This physics interface describes the current and potential distribution in an electrochemical cell under the assumption that the conductivity of the electrolyte can be assumed constant, so that charge transport obeys Ohm's law. Under this assumption, variations in electrolyte composition due to the electrochemical reaction are negligible. Migration of ions gives the only net contribution to the current in the electrolyte. The secondary case does account for activation losses which are caused by the slowness of the reactions taking place on the electrode surface. The relation between charge transfer and overpotential can be described using arbitrary kinetic expressions, such as Butler-Volmer and Tafel equations.

Both Primary and Secondary Current Distributions treat the electrolyte current as Ohmic, and solve only for electrolyte potential for a given conductivity, assuming the electrolyte composition to be negligibly perturbed by electrolysis or current flow. However, Primary Current Distribution neglects the activation losses due to charge transfer reactions and this is the difference from the Secondary Current Distribution. In addition, Tertiary Current distribution, describes the current and potential distribution in an electrochemical cell, taking into account the transport of ions in the electrolyte through diffusion, migration and convection. Finally, the Electroanalysis interface assumes the presence of excess supporting electrolyte and so predicts a current–voltage relation by solving the diffusion–convection equation for the electro-active species.

6.4 Model inputs

6.4.1 Introduction

This thesis deals with the use of steel in shipbuilding and in particular with the phenomenon of the AH36 and S690 steel general corrosion in simulated marine environment (solution NaCl 3.5%). An electrochemical model has been created in Comsol so as to simulate the experimental procedure of the above mentioned steels (chapter 5).

The Secondary Current Distribution is the solution method which used for developing this model because it does account for activation losses which are caused by the slowness of the reactions taking place on the electrode surface. The relation between charge transfer and overpotential can be described using arbitrary kinetic expressions, Butler-Volmer (eq. 6.1) and Tafel (eq. 6.2) equations.

$$i_{corr} = i_o\left(\exp\left(\frac{\alpha_\alpha F\eta}{RT}\right) - \exp\left(\frac{-\alpha_c F\eta}{RT}\right)\right) \quad (6.1)$$

$$\eta = \beta\, log\frac{i}{i_{corr}} \quad (6.2)$$

Consequently, this physics interface describes the current and potential distribution in an electrochemical cell under the assumption that the conductivity of the electrolyte can be assumed constant, so that charge transport obeys Ohm's law (eq.6.3). Under this assumption, variations in electrolyte composition due to the electrochemical reaction are negligible. Migration of ions gives the only net contribution to the current in the electrolyte.

$$I = \frac{E}{R} \quad (6.3)$$

6.4.2 Model Definition

For the simulation of the experiments, the development of 1D model was selected as presented in *Figure 26*. The 2D model would provide more information on the distribution of current on the electrode surface, as well as the distribution of potential in the electrolyte. However, since the aim of the model is to simulate the polarization curves, the development of 1D model is sufficient. The designed geometry represents a half-cell which is a structure that contains a conductive electrode and a surrounding conductive electrolyte. Chemical reactions occur between the electrode and the electrolyte, resulting in a potential difference between them.

The simulated electrochemical cell consists of two electrodes:

1. The electrolyte electrode interface which represents the working electrode (point 1-*Figure 26*)
2. The boundary electrolyte potential which represents the reference electrode (point 2-*Figure 26*)

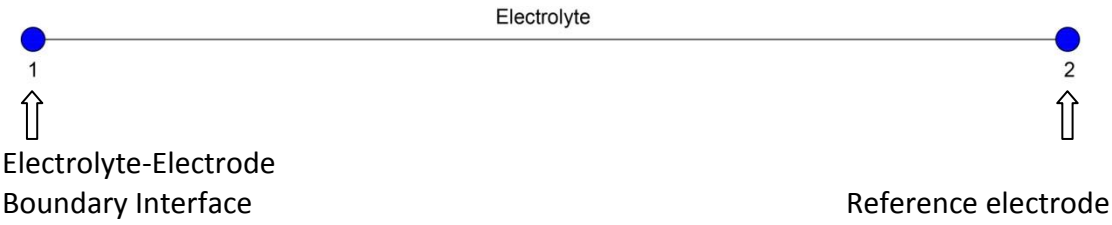

Figure 26: Half cell as 1D geometry

As metal electrode, is defined AH36 or S690 steel, so as to assess their susceptibility for corrosion. Each material, is described from its equilibrium potential (E_{eq}) because of of their different chemical composition and microstructure. Thus, the E_{eq} of the specimens which used for the experimental procedure, is -0.700 V and -0.670 V for AH36 and S690 steel, respectively.

The simulated electrochemical cell consists of two electrodes: the working electrode (point 1): the electrolyte electrode interface, and the reference electrode

(point 2): boundary electrolyte potential. As reference electrode is used Saturated Calomel Electrode (SCE) at the outer electrolyte boundary (point 2). SCE is the most common reference electrode used for experiments. Its electrode potential is $E_{cal} = 0.240V$ vs. hydrogen electrode.

In order to build up the electrochemical model, by the selected solution method Secondary Current Distribution, the following parameters need to be defined (*Figure 27*):

1. **Electrolyte**. The domain of the 1D geometry is defined to be the electrolyte. The solution used in the experiments is NaCl 3.5% w/w. According to the literature the value of the conductivity of this electrolyte is σ=500 S/m.

2. **Electrolyte Potential**. The second boundary (point 2) accounts for the boundary electrolyte potential: $\Phi_{l,bnd} = -0.240$V. This value is in accordance with the potential Saturated Calomel electrode which is SCE= +240V vs. Hydrogen electrode.

3. **Electrolyte-Electrode Boundary Interface.** On this Boundary (point 1) is where all the reactions between Electrolyte and Electrode take place. There are many reactions that occur at this point. However, is selected to be examine the reactions below:

Fe $\rightarrow Fe^{2+} + 2e^-$	Anodic - Oxidation
$2H^+ + 2e^- \rightarrow H_2$	Cathodic - Reduction
$O_2 + 2H_2O + 4e^- \rightarrow 4OH^-$	Cathodic - Reduction

The above parameters (1,2,3) are described in detail in the following paragraphs.

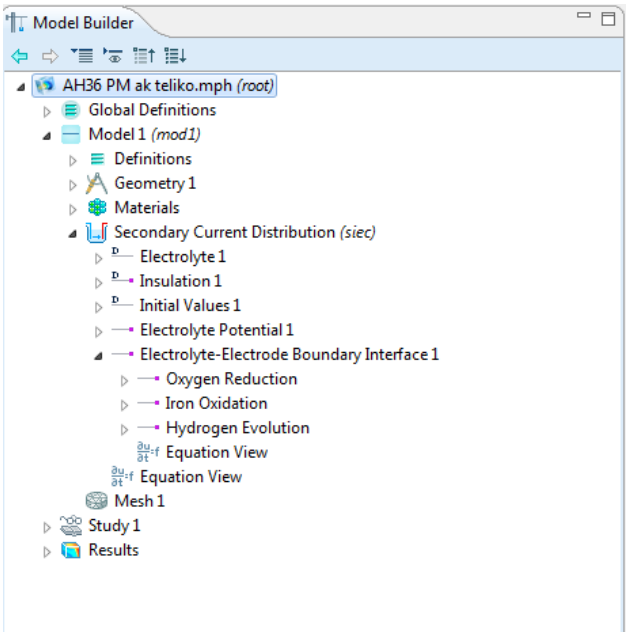

Figure 27: Secondary current distribution is selected as the solution method.

1. Electrolyte - Domain definitions

We assume the presence of an electrolyte quantity of NaCl 3.5%w/w with electrolyte conductivity σ=500 S/m in order to simulate the seawater environment.

Assuming electroneutrality and negligible concentration gradients of the ions, the following expression describes the current density vector in the electrolyte.

$$i_l = -F^2 \sum z_i^2 u_{m,i} c_i \nabla \Phi_l \quad (6.1)$$

Moreover, if we assume approximately constant composition of charge carriers, we can define a constant electrolyte conductivity as:

$$\sigma_l = F^2 \sum z_i^2 u_{m,i} c_i \quad (6.2)$$

Thus, the current density in the electrolyte can be written as:

$$i_l = -\sigma_l \nabla \Phi_l \quad (6.3)$$

2. Electrolyte Potential – Point 2

At this boundary is defined the reference electrode in accordance with the experimental procedure. So, Saturated Calomel Electrode (SCE) is determined as reference electrode at the outer electrolyte boundary (point 2). Its electrode potential is $E_{cal} = 0.240V$ vs. hydrogen electrode.

The boundary condition for the electrolyte potential is the following:

$$\Phi_l = \Phi_{l,bnd}$$

Where, $\Phi_{l,bnd} = -0.240V$. This value is in accordance with the potential Saturated Calomel electrode which is SCE= +240 vs. Hydrogen electrode.

3. Electrolyte-Electrode Boundary Interface – Point 1

Electrolyte-Electrode Domain Interface is a boundary condition that describes the electrochemical interface between the electrode and the electrolyte domain (*Figure 28*). At this Boundary is defined the above mentioned reactions between Electrolyte and Electrode.

Fe $\rightarrow Fe^{2+} + 2e^-$	Anodic - Oxidation
$2H^+ + 2e^- \rightarrow H_2$	Cathodic - Reduction
$O_2 + 2H_2O + 4e^- \rightarrow 4OH^-$	Cathodic - Reduction

The above electrode reactions can be described using arbitrary electrode kinetic expressions of the overpotential for the anodic and cathodic cases. At the working electrode surface (point 1-Electrolyte-Electrode Boundary Interface), the iron (Fe) is dissolved (anodic reaction) to the electrolyte. The mathematical background of this procedure is described in the following paragraphs.

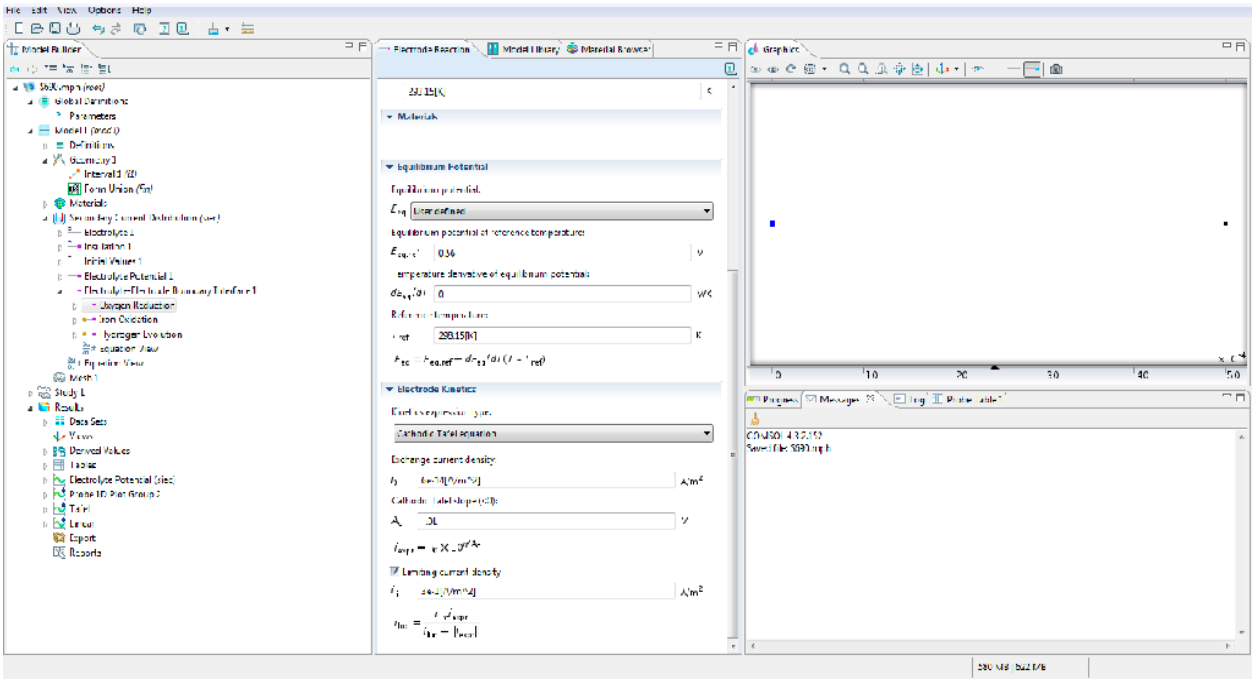

Figure 28: Definition of the chemical reactions

The current density for these reactions is given by the electro-analytical Butler-Volmer equation:

$$i_{corr} = i_o\left(\exp\left(\frac{\alpha_\alpha F\eta}{RT}\right) - \exp\left(\frac{-\alpha_c F\eta}{RT}\right)\right) \quad (6.4)$$

In which, α_α & α_c is the anodic and cathodic transfer coefficient respectively, and η is the overpotential at the working electrode. The overpotential is the difference between the applied potential ($\Phi_{s,ext}$), the potential of electrode's response to the applied potential (Φ_l) and the equilibrium potential (E_{eq}) of the redox couple of species:

$$\eta = \Phi_{s,ext} - \Phi_l - E_{eq} \quad (6.5)$$

$\Phi_{s,ext}$ is the a time depended applied potential. $\Phi_{s,ext}$ is determined as $\Phi_{s,ext} = -1 + 0.01t$ because the initial point for the potential sweep (t=0) is equal to -1000mV. The potential sweep starts from the cathodic area and proceeds to anodic area with time step 0.01mV/s. For consistency with the experimental procedure the maximum applied potential is approximately -450mV and the required time is 50s.

The Butler-Volmer relationship for current density is based on identifying the anodic and cathodic reactions that are taking place on each electrode. In any environment a metal is undergoing both anodic and cathodic reaction. This characteristic is what requires the net current density to account for both reactions on each metal, regardless of if the metal is acting as the anode or the cathode in a galvanic couple. At the equilibrium potential (zero overpotential) the anodic and cathodic currents are equal, this point is known as the exchange current. However, when the overpotential is not equal to zero, the anodic and cathodic currents are different. Hereafter, is described the definition of the three chemical reactions of the model:

- **Iron Dissolution (Anodic reaction)**

In case of iron immersed in a solution NaCl 3.5% (electrolyte), iron is dissolves Fe^{2+} ions in the solution, so this reaction is anodic and is described as follows:

$$\text{Fe} \rightarrow Fe^{2+} + 2e^{-}$$

The overpotential, η, is given according to the following equation:

$$\eta = \Phi_{s,ext} - \Phi_{l} - E_{eq} \quad (6.5)$$

Where E_{eq} is depended from the composition of the steel. In this case -0.700V and -0.670V for AH36 and S690 steel, respectively.

Anodic Tafel equation is selected for Fe dissolution. So the i_{corr} is given by the anodic part of the electro-analytical Butler-Volmer equation (6.4):

$$i_{corr} = i_0 \times 10^{\eta/A_a} \quad (6.6)$$

For consistency with the experimental procedure:

$$\mathrm{i_0} = 0.5\mathrm{x}10^{-4}\ \mathrm{A/m^2} \text{ and } \mathrm{A_a} = 0.055\mathrm{V}$$

- **Oxygen Reduction (Cathodic reaction)**

When an electrolyte solution is exposed to the atmosphere, it contains dissolved oxygen. In this case we have a decrease in oxidation state so the reaction is cathodic and is defined below:

$$O_2 + 2H_2O + 4e^- \rightarrow 4OH^-$$

The overpotential, η, is according to the following equation:

$$\eta = \Phi_{s,ext} - \Phi_l - E_{eq} \quad (6.5)$$

According to the literature, the E_{eq} of oxygen is 0.820V. Since in the experiment Saturated Calomel Electrode is used as reference electrode, the Equilibrium potential of oxygen is:

$$E_{eq} = 0.820 - 0.240 = 0.560\text{V}$$

After that, is defined the solution method for the above reaction. So, in Electrode Kinetics type we choose Cathodic Tafel equation because we have a decrease in oxidation state. So, the i_{corr} is given by the electro-analytical Butler-Volmer equation (6.4):

$$i_{corr} = -i_0 x 10^{\eta/A_c} \quad (6.7)$$

For consistency with the experimental procedure:

$$\mathrm{i_0} = 6\mathrm{x}10^{-13}\ \mathrm{A/m^2} \text{ and } \mathrm{A_c} = -0.010\mathrm{V}$$

Limited current density has been taken into account according to

$$i_{corr} = \frac{i_{lim} i_{expr}}{i_{lim} + \|i_{expr}\|} \quad (6.8)$$

Where, $i_{lim} = 3x10^{-1}\ \mathrm{A/m^2}$.

- **Hydrogen Evolution (Cathodic reaction)**

There are many cathodic reactions involving in the corrosion of metals, according to the corrosive environment. Hydrogen evolution is one of the most common.

$$2H^{+} + 2e^{-} \rightarrow H_2$$

The overpotential, η, is according to the following equation:

$$\eta = \Phi_{s,ext} - \Phi_l - E_{eq} \quad (6.5)$$

According to the literature, the E_{eq} of hydrogen is -0.83V.

Cathodic Tafel equation is selected as solution method. So the i_{corr} is given by the cathodic part of the electro-analytical Butler-Volmer equation (6.4):

$$i_{corr} = -i_0 x 10^{\eta/A_c} \quad (6.9)$$

For consistency with the experimental procedure:

$$\mathrm{i_0 = 10\ A/m^2} \ \text{ and } \ \mathrm{A_c = -0.060V}$$

Having defined all the necessary parameters and equations for the model, Comsol gives the Tafel curve of the steel as it depicted in *Figure 29*.

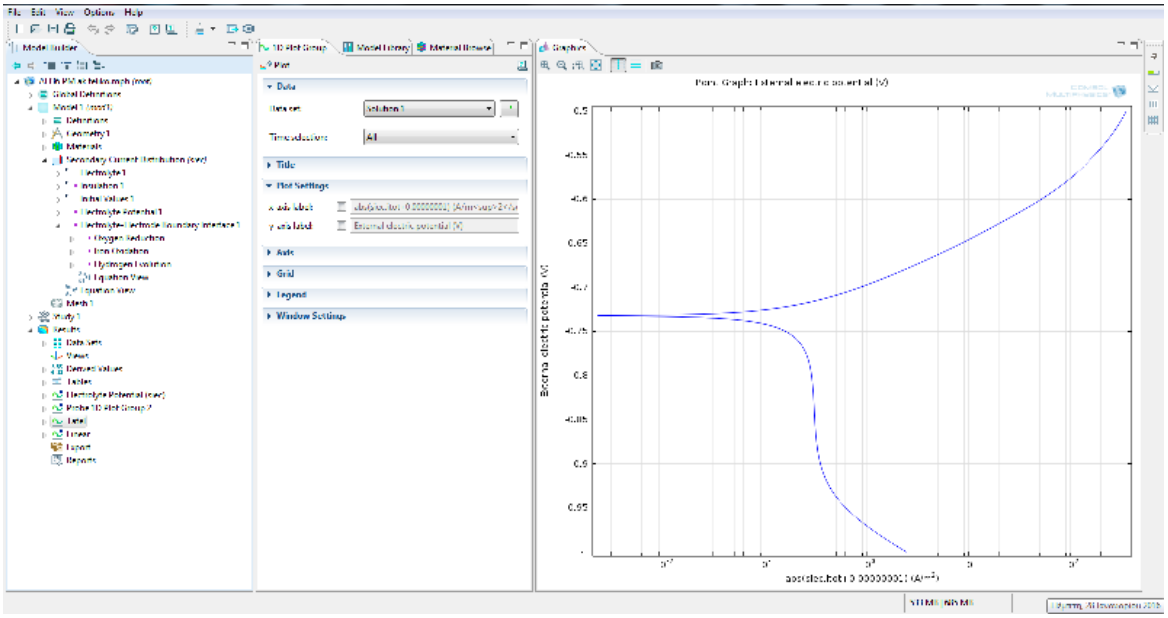

Figure 29: Tafel curve of AH36.

7. RESULTS

This chapter presents the Tafel curves as they derived from the modelling with Comsol Multiphysics software taking into the experimental results presented in chapter 5. The potentiodynamic polarization curve, is one of the most common methods of examining the corrosion behaviour of materials. After the simulation of the experimental process, the outcomes are compared to the experimental results. According to these curves can be received very useful information about the corrosion resistance of the steels as well as the verification and validation of the simulating method.

7.1. Results for AH36 steel

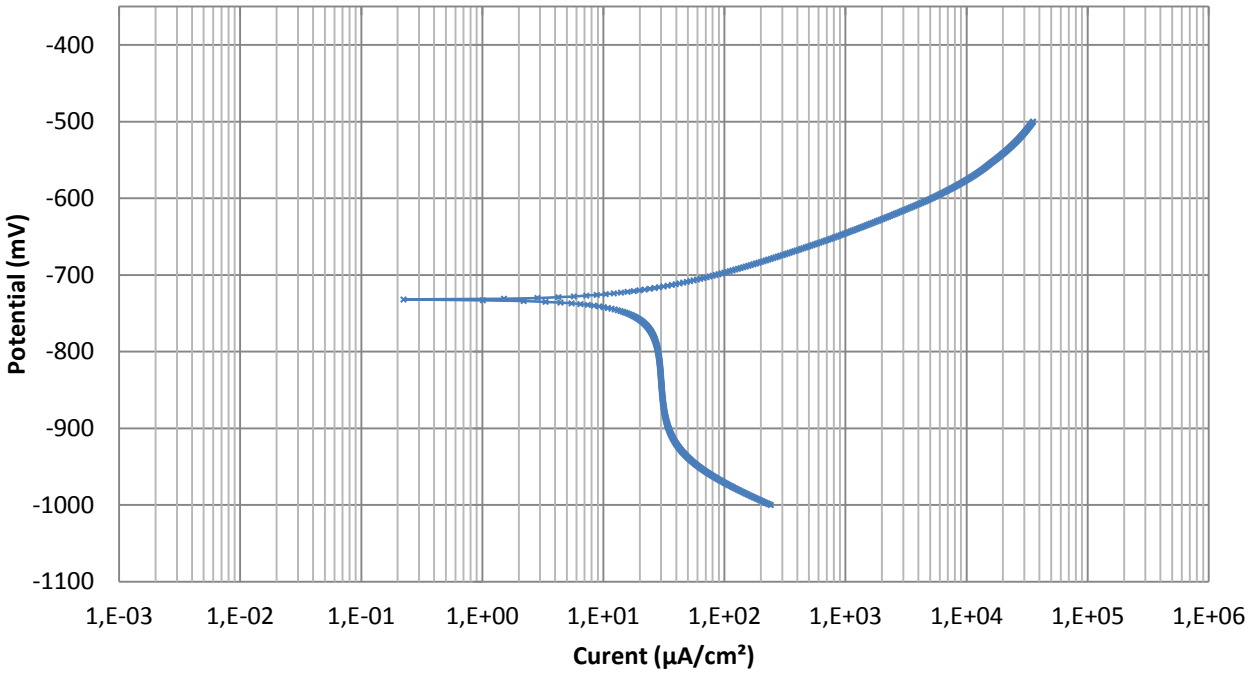

Figure 30: Simulated Polarization curve of AH36 steel.

The above Tafel curve (*Figure 30*) is generated by the polarization of the AH36 steel using the Tafel extrapolation method for ±250mV vs. E_{eq}. The Corrosion potential $E_{corr} = -740$ mV while the corrosion rate is i_{corr} =2x10 μA/cm^2. According to the

model definition the anodic part represents the iron oxidation (anodic reaction) while the cathodic, is the combination of the oxygen reduction and hydrogen evolution (cathodic reactions).

The polarization curve, as shown in *Figure 31*, is a comparison between the polarization curves derived from experimental procedure of AH36 steel and from the simulation model in order to examine the validation of the modelling procedure. The validation work consists of experimental determination of electrochemical data which can be compared with the results of the computational modelling.

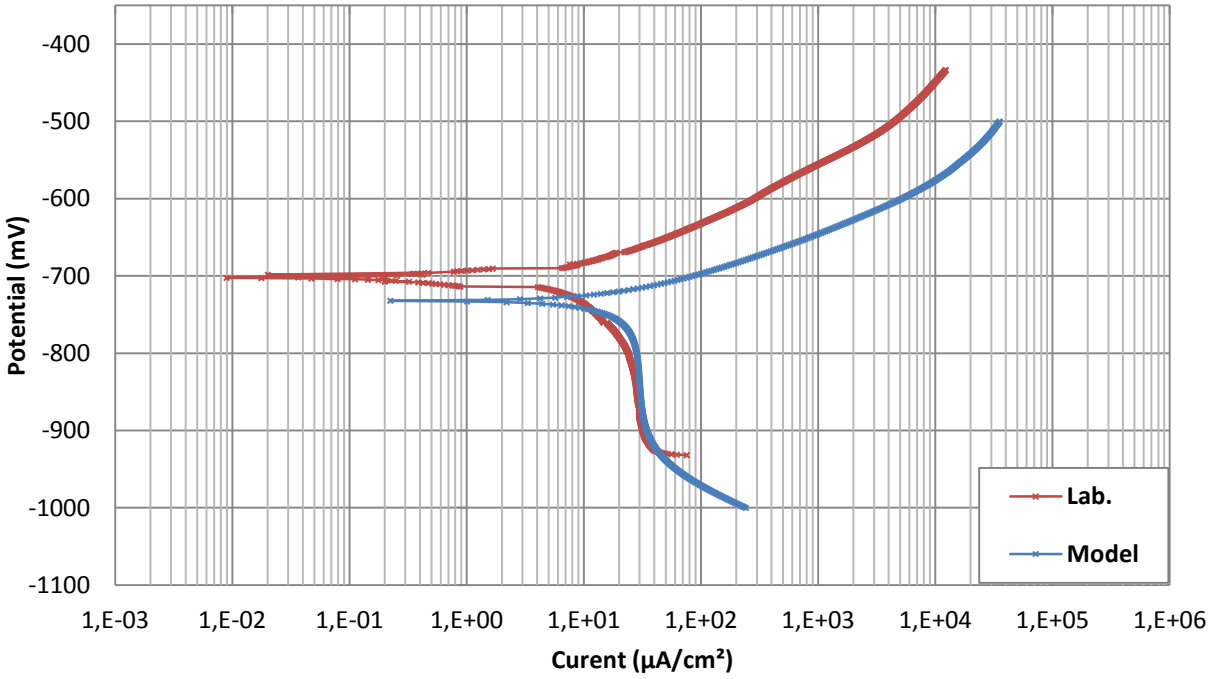

Figure 31: Comparison between experimental measurements and simulation results for AH36 steel.

According to *Figure 31*, it can be observed that the difference between experimental and simulated curve is negligible. As a result, it can be concluded that the model developed using the software Comsol is able to simulate rather well the experimental procedure.

7.2 Results for S690 steel

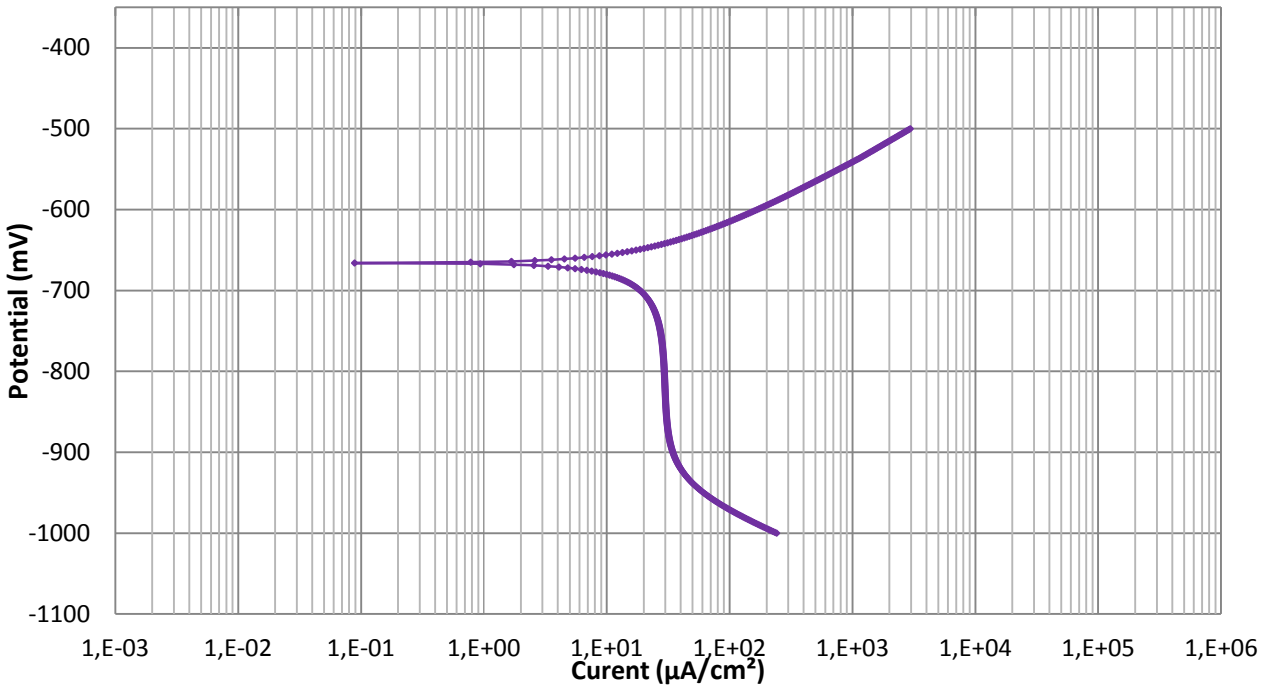

Figure 32: Simulated Polarization curve of S690 steel.

The Tafel curve (*Figure 32*) is generated by the polarization of the S690 steel using the Tafel extrapolation method for ±250mV vs. E_{eq}. The Corrosion potential for this material is $E_{corr} = -660$ mV while the corrosion rate is approximately i_{corr} =2x10μA/cm^2.

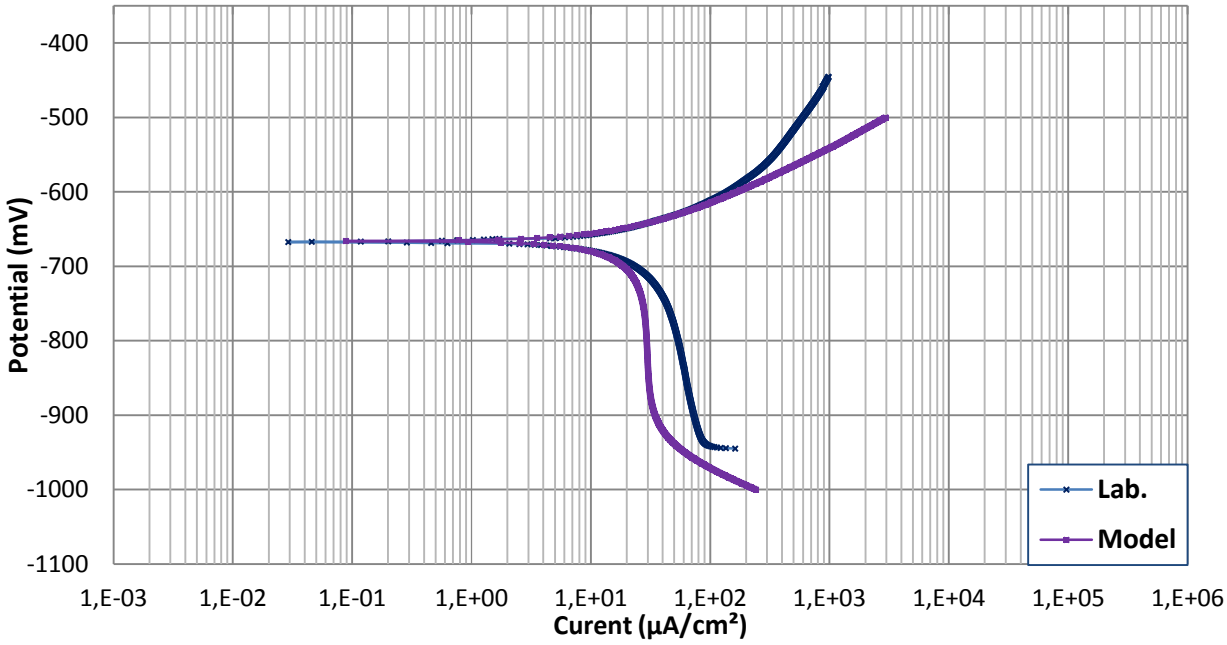

Figure 33: Comparison between experimental measurements and simulation results for S690 steel.

The comparison between the experimental part and the simulation model of S690 steel is shown in *Figure 33*. In this case, the E_{corr} and i_{corr} of the two curves are in conformity. Consequently, the experimental measurements and the simulated results are in very good agreement.

From the Tafel curves above, it is concluded that the approach and the solution method which chosen in order to simulate the experimental procedure is valid. The decision to select the reactions of Iron oxidation, Oxygen reduction and Hydrogen evolution proved to be right. So, we accomplished the elucidation of the main anodic and cathodic reaction that determines the electrochemical experiments.

7.3 Simulated polarization curves of AH36 – S690 steels.

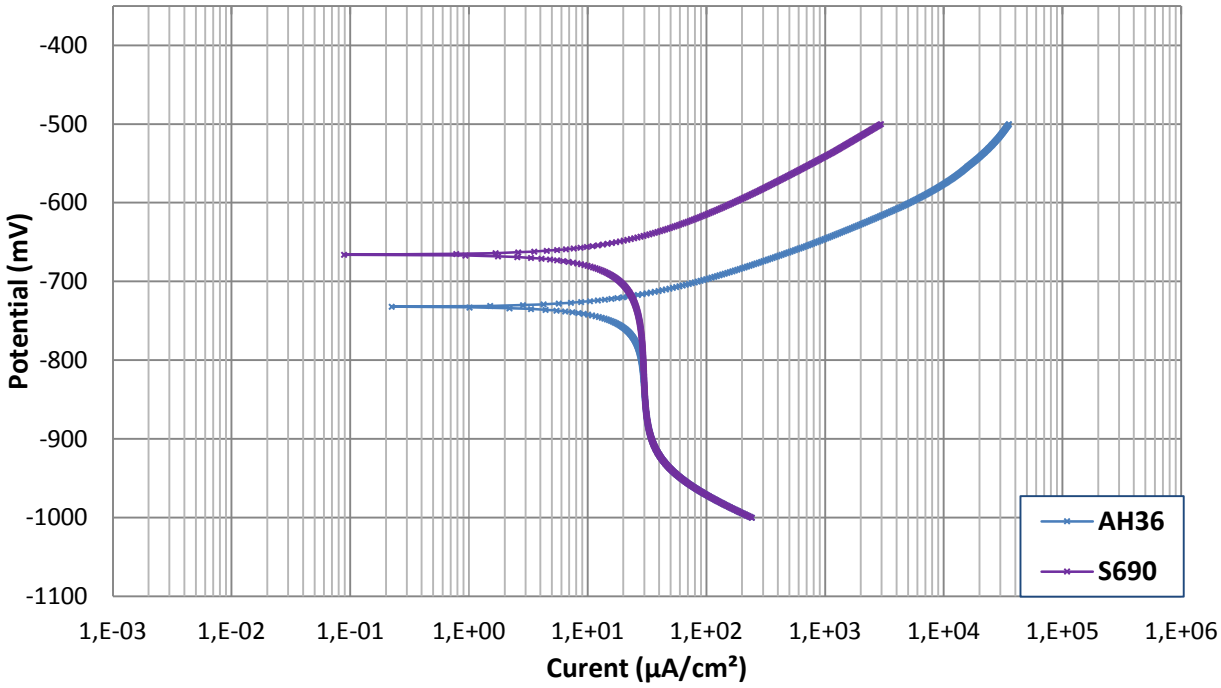

Figure 34: Comparison between simulated polarization curves of AH36 – S690 steels.

The Tafel curves of the two different metals, *Figure 34*, present a slight difference in the E_{corr}, -740mV & -660mV for the AH36 and S690 steel respectively. Thus, E_{corr} is lower for AH36 resulting that AH36 is more active to corrosion. However the values for the corrosion current i_{corr}, is rather similar, implying that the corrosion rate is similar for the two different metals. These conclusions are in agreement with the comparison between the experimental measurements of the two kinds of steels.

7.4 Potential Distribution in the electrolyte

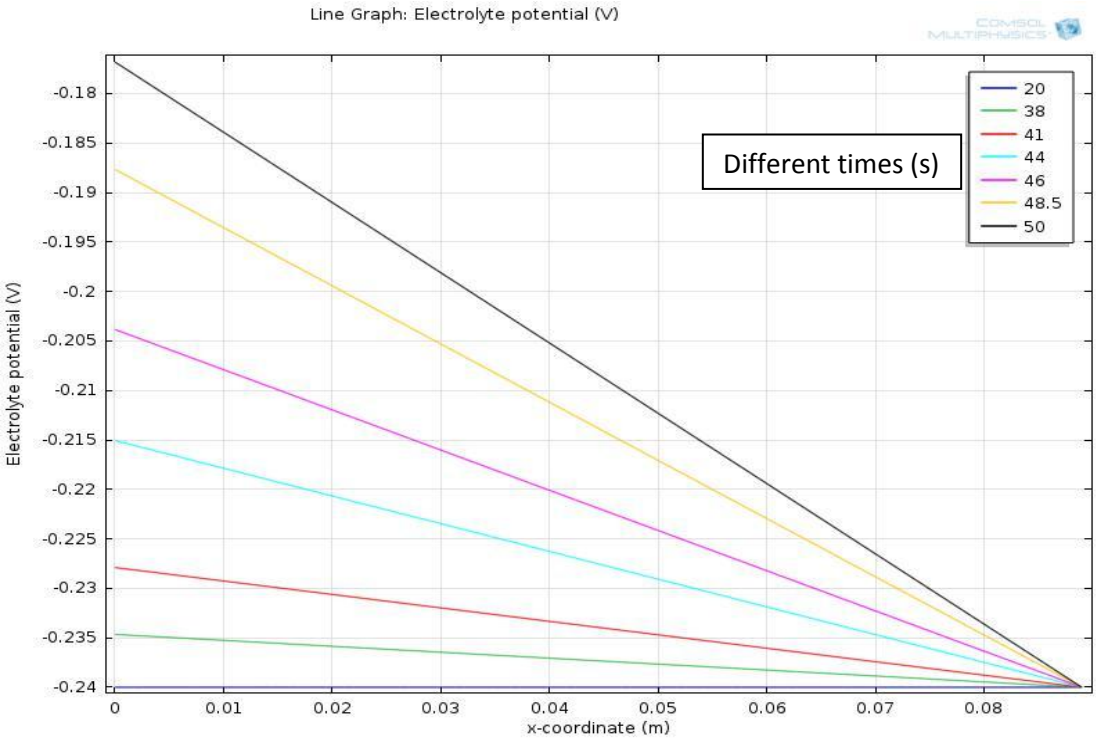

Figure 35: Potential distribution in the electrolyte for AH36 steel, in different times.

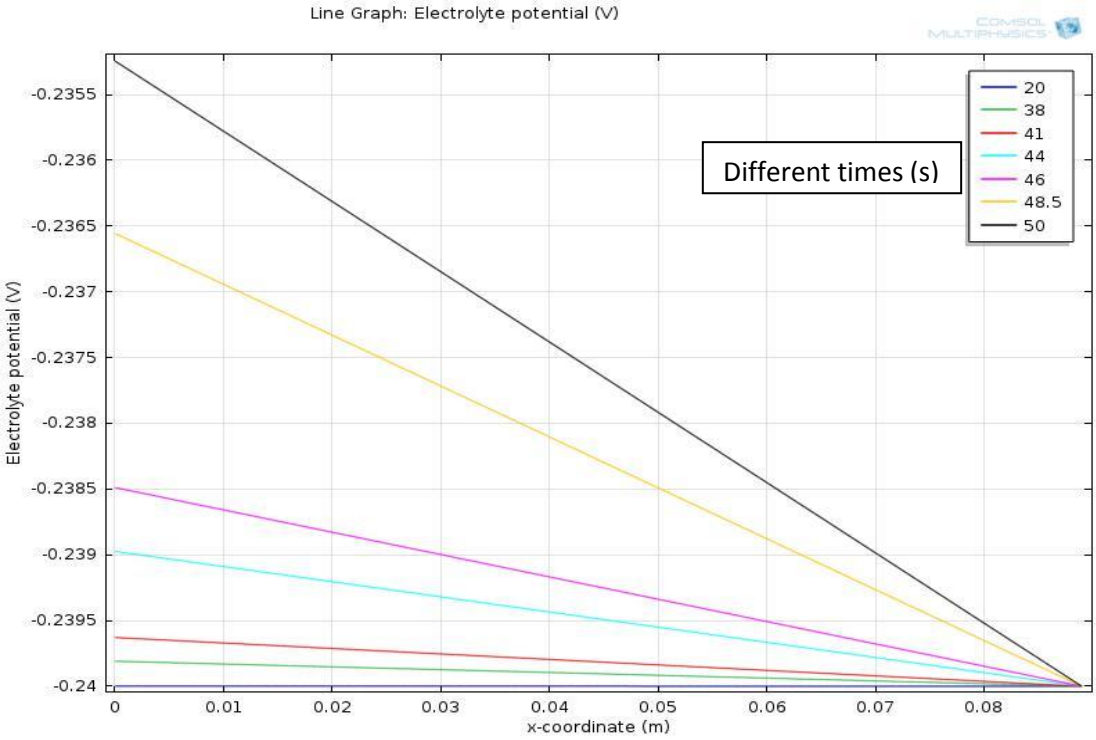

Figure 36: Potential distribution in the electrolyte for S690 steel, in different times.

The previous figures, (*Figure 35, Figure 36*) present the change of the electrolyte potential in the half cell in different times because of the dissolution of the metal in the solution. Specifically, x-axis represents the cell size in where x=0 is at point 1 and x=0.89 is the point 2. For t=0 the potential is the same in all the solution as it does not happens any change inside it, so for t=0 the electrolyte potential is a straight line parallel to x-axis. After that, when the polarization of the steels begins, the electrolyte potential is getting changed because of the metal dissolution (cations of the metal, released in the solution).

The potential change is linear from point 1 of the model to point 2 and the slope of the lines is time dependant. The linearity of the above curves proves that the electrolyte solution is a typical Ohmic solution. This observation verifies the selection of secondary current distribution method for the model development.

7.5 Model development for Deaerated solution

Taking into account the experimental result and the model development in the previous paragraphs, the simulation of the phenomenon in deaerated solution was decided. The following Tafel curves depict the behavior of the steels without the oxygen reaction. In order to evaluate the corrosion susceptibility in deaerated NaCl 3.5% solution, we developed the model taking into account only the iron oxidation as anodic reaction and hydrogen evolution as cathodic one. The results are presented in the following figures (*Figure 37, Figure 38*).

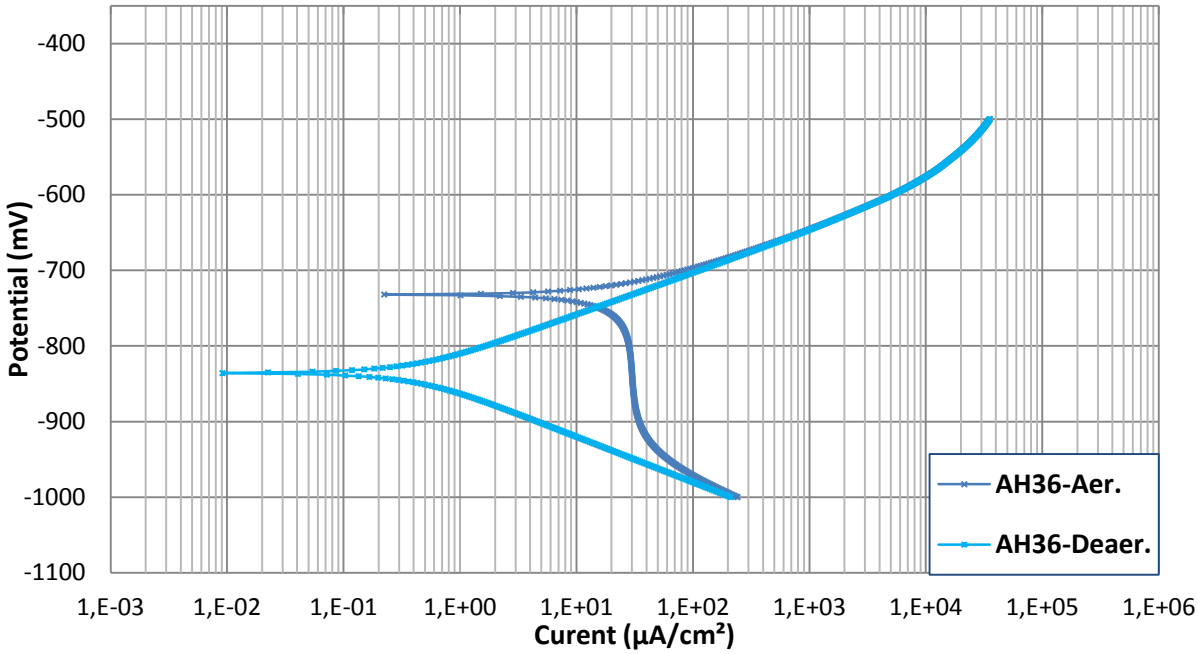

Figure 37: Comparison between Tafel curves of AH36 in aerated and deaerated solution.

The curve in *Figure 37* presents the corrosion behavior of the AH36 steel in deaerated solution in comparison to aerated one. In the case of deaerated solution the $E_{corr} = -840mV$ and the $i_{corr} = 2x10^{-1}$ μA/cm^2 while in aerated solution $E_{corr} = -740mV$ and the $i_{corr} = 2x10$ μA/cm^2. Comparing these measurements it can be concluded that in deaerated solution the corrosion potential and corrosion rate are decreased, so the steel has better corrosion behavior than in aerated solution. This confirms that in both solution methods (experimental-simulated), the phenomenon is mainly controlled by the oxygen reduction.

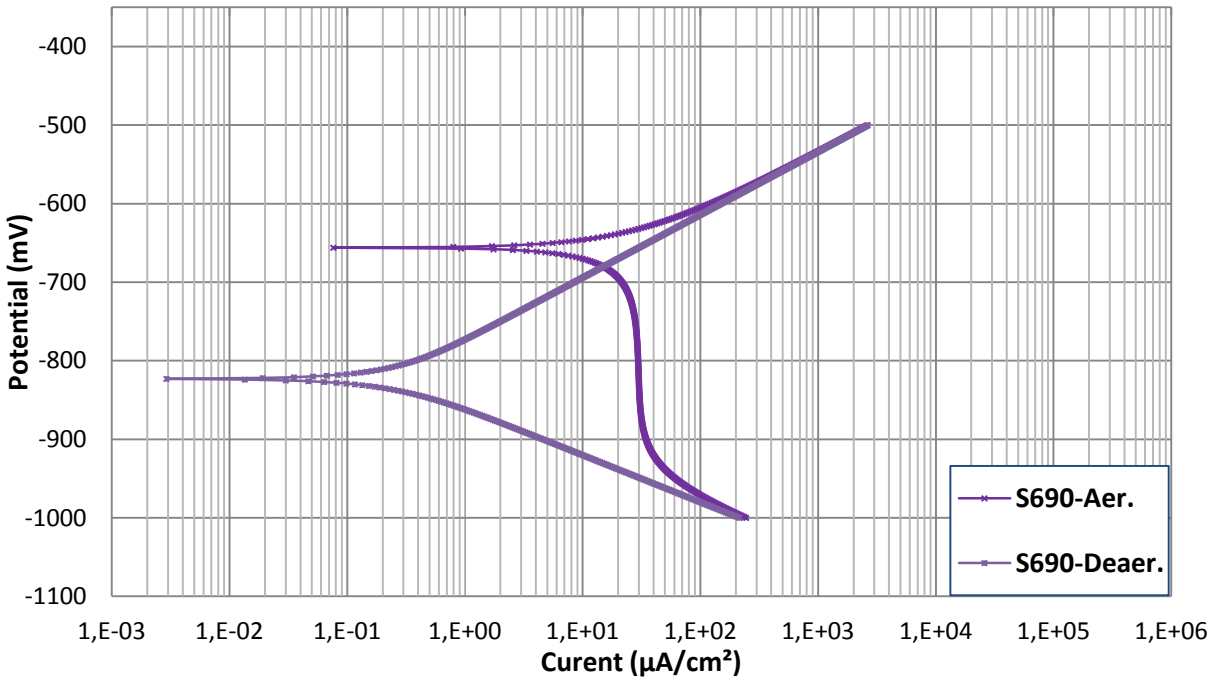

Figure 38: Comparison between Tafel curves of S690 in aerated and deaerated solution.

The same conclusions are observed for the S690 steel *Figure 38*. In this case the $E_{corr} = -820mV$ and the $i_{corr} = 1x10^{-1}$ μA/cm^2 in deaerated solution, while in aerated solution $E_{corr} = -670mV$ and the $i_{corr} = 10$ μA/cm^2.

The previous curves (*Figure 37*, *Figure 38*) verify that the phenomenon is mainly controlled by the reduction of oxygen in the solution as the corrosion behavior in both cases, is better in deaerated solution than in aerated one.

CONCLUSIONS

The aim of the present thesis is the Polarization curves modelling concerning the corrosion behavior of naval steels and experimental validation. This was accomplished through experimental electrochemical testing where polarization curves were obtained and consequently 1D model was developed employing Comsol Multiphysics 4.3b software for the simulation of the polarization curves and the validation of the experimental results.

The electrochemical experiments resulted in polarization curves, where The Tafel curves for metals present a slight difference in the corrosion potential E_{eq}, lower for AH36, thus from thermodynamic point of view, AH36 is more active to corrosion. However, the values for the corrosion current i_{corr}, is rather similar, implying that the corrosion rate is similar for the two different metals. Moreover the shape of the cathodic part of the curve shows that the phenomenon is controlled by the reduction of oxygen.

Employing the Electrochemistry Module of Comsol Multiphysics 4.3.b, a 1D model was developed for the simulation of the experimental polarization curves. For the 1D model, Secondary current distribution for the electrochemical phenomenon was assumed, and Butler-Volmer and Tafel equations were applied for the solution of the problem. Moreover, concerning the electrochemical reaction which take place in the present experiments, Fe dissolution, hydrogen evolution and oxygen reduction were also assumed.

Considering the results obtained from the experimental and the simulation process, it can be concluded that they are in good agreement as the difference between experimental and simulated curves is negligible for both AH36 and S690 steels. It is proved that the approach and the solution method which were chosen in order to simulate the experimental procedure, is valid. Moreover, the reactions assumed: Fe dissolution, hydrogen evolution and oxygen reduction so as to simulate the experimental procedure, proved to be right. Hence, it is accomplished the elucidation of the main anodic and cathodic reaction that determines the electrochemical experiments.

From the model developed the electrolyte potential curves obtained for different times, proved that the electrolyte solution is an Ohmic one.

Besides, the simulation of the phenomenon, employing the model developed, provided useful results concerning their behavior in deaerated solution. The polarization curves obtained proved that AH36 and S690 steels, present better corrosion behavior than in aerated solution. This confirms that in both solution methods (experimental-modelling), the phenomenon is mainly controlled by the oxygen reduction.

FUTURE CHALLENGES

To meet future challenges for shipbuilding corrosion protection systems arising from new kind of materials and material combinations (new generations of metal alloys, material made from renewable resources etc), the following are some of the needs for future generation of shipbuilding:

- Experimental investigations used in combination with chemical and physical modelling approaches utilizing feedback from actual data.
- The usage and combination of numerical tools in a sensible way.
- Rigorous definition and implementation of procedures and criteria for verification, validation and accreditation of modeling methods to increase the likelihood of their acceptance and use for shipbuilding certification.
- Involve more and more material suppliers in the development work of relevant corrosion modeling and simulation.

Simulations in chemical reaction engineering are used for different reasons during the investigation and development of a reaction process or system. In the initial stages, they are used to dissect and understand the process or system. By setting up a model and studying the results from the simulations, engineers and scientists achieve the understanding and intuition required for further innovation.

Once a process is well understood, modelling and simulations are used to optimize and control the process' variables and parameters. Another use for modeling is to simulate scenarios that may be difficult to investigate experimentally. One example of this is to improve safety, such as when an uncontrolled release of chemicals occurs during an accident. Simulations are used to develop protocols and procedures to prevent or contain the impact from these hypothetical accidents.

In all these cases, the development of reliable models and simulations is an essential part of future predictive maintenance concepts and provide value for money by reducing the need for a large number of experiments or to build prototypes, while, potentially, granting alternate and better insights into a process or design.

REFERENCES

[1] Abílio M.P. de Jesus, Rui Matos, Bruno F.C. Fontoura, Carlos Rebelo, Luis Simões da Silva, Milan Veljkovic.(2012). *A comparison of the fatigue behavior between S355 and S690 steel grades.* Sweden-Portugal.

[2] Christopher D. Taylor. (2012). *Atomistic Modeling of Corrosion Events at the Interface between a Metal and Its Environment.*

[3] Comsol 2013*, Impressed Current Cathodic Protection of a Ship Hull, Solved with* Comsol *Multiphysics 4.3b, 2013.*

[4] Comsol *2013, Corrosion Protection of an Oil Platform Using Sacrificial Anodes, Solved with* Comsol *Multiphysics , 2013.*

[5] Comsol 2013. *Simulation of Electrochemical Impedance Spectroscopy.* Solved with Comsol Multiphysics *4.3b* 2013

[6] Comsol 2013. *Cathodic Protection of Steel in Reinforced Concrete.* Solved with Comsol Multiphysics *4.3b* 2013

[7] Denny A. Jones. (1996). *Principles and Prevention of Corrosion.* U.S.A: Prentice Hall.

[8] Daniel Sebastia-Saez, Sai Gua, Panneerselvam Ranganathana ,Konstantinos Papadikis.(2014). *Micro-scale CFD modeling of reactive mass transfer in falling liquidfilms within structured packing materials.UK.*

[9] En.wikipedia.org

[10] H. TAN (2002) *Combined Atomistic and Continuum Simulation of Fracture and Corrosion* Louisiana State University, Baton Rouge, LA, USA.

[11] Jian Hua n , Chih-Wen Cheng*. Corrosion of high tensile steel onboard bulk carrier loaded with coal of different origins*, Department of Marine Engineering, National Taiwan Ocean University, Keelung City. Taiwan.

[12] J.A. DeRose, T. Suter, T.Hack, R.A. Adey,(2013). *Corrosion of aircraft Structures Modelling and Simulation.*U.S.A: WIT Press

[13] J.C.Scully. (1975). *The Fundamentals of Corrosion*. England.

[14] Klaus Capelle. (2006). *A Bird's-Eye View of Density-Functional Theory.* Brazil.

[15] Καραντώνης. Α. (2010). Βασικές Αρχές Ηλεκτροχημείας. Αθήνα.

[16] L.C. Abodi, O.Guseva, J.A. DeRose. (2013). *Modelling of the Aluminium Alloy AA2024 at the Microscale: Pitting and Intergranular Corrosion.Switzerland-Belgium.*

[17] Μπάκας Α.(2015). *Μελέτη της μικροδομής και της συμπεριφοράς σε διάβρωση συγκολλήσεων τόξου και υβριδικών συγκολήσεων Lases-Τόξου.* Διπλωματική εργασία, ΕΜΠ.

[18] Nestor Perez. (2004). *Electrochemistry and Corrosion Science.* Bonston: Kluer Academic Publishers.

[19] Παντελής Δ.Ι., Τσιούρβα Θ. (2006). *Διάβρωση και προστασία ναυπηγικών χαλύβων.* Αθήνα.

[20] R.G.Kelly, D.Shoedmith, R.G.Bunchheit. (2003). *Electrochemical Techniques in Corrosion Science and Engineering.* U.S.A

[21] R.Adey,T.Hack, A.Peratta, S. Palani, H.Lohner.(2013). *Macroscale Galvanic Corrosion Modelling of an Aluminium Alloy*. Germany.

[22] R.A.Ricks, P.R.Howell G.S. Barritte. (1982). *The nature of acicular ferrite in HSLA steel weld metals.*UK.

[23] R. Oltra, A. Zimmer, J.Deconinck.(2013). Modelling of an Aluminium Alloy at the mesoscale: Crevice Corrosion.Belgium

[24] S. Beretta, A. Bernasconi, M. Carboni.(2008). *Fatigue assessment of root failures in HSLA steel welded joints: A comparison among local approaches.* Politecnico di Milano, Italy.

[25] Xuhong Qiang, Frans Bijlaard, Henk Kolstein.(2011). *Dependence of mechanical properties of high strength steel S69 on elevated temperatures*. Delft, University of Technology.